CURRENT COLLECTION IN A MAGNETOPLASMA

J.G. Laframboise and L.J. Sonmor

Physics Department, York University
Downsview, Ontario, Canada M3J 1P3

ABSTRACT

We present a survey of a very incomplete subject. Our presentation is intended in part as an introduction to topics to be covered in greater detail by others later in this Workshop. The best-developed and simplest theories for current collection are steady-state collisionless theories, and these must be understood before departures from them can be analyzed usefully, so we begin with a review of them. We include some recent numerical results by one of us (L.J.S.) which indicate that steady-state collisionless Laplace-limit currents remain substantially below the Parker-Murphy (1967) canonical upper bound out to very large electrode potentials, and approach it as a limit only very slowly if at all. Attempts to correct this theory for space-charge effects lead to potential disturbances which extend to infinite distance along the electrode's magnetic shadow, unless collisional effects are also taken into account. However, even a small amount of relative plasma drift motion, such as that involved in a typical rocket experiment, can change this conclusion fundamentally. It is widely believed that time-averaged current collection may be increased by effects of plasma turbulence, and we review the available evidence for and against this contention. Steady-state collisionless particle dynamics predicts the existence of a toroidal region of trapped orbits which surrounds the electrode. Light emissions from this region have been photographed, indicating that collisional ionization may also occur there, and this, and/or scattering by collisions or possibly turbulent fluctuations in this region, may also increase current collection by the electrode. We also discuss effects on particle motions near the electrode, associated with "breakdown of magnetic insulation" in the region of large electric fields near it.

1. INTRODUCTION

Even without magnetic-field effects, the problem of predicting current collection by objects ("probes") in plasmas is one of the most formidable in plasma physics. Reasonably complete solutions of it exist only for very simple geometries, in the limits of large and small mean-free-paths, and in the absence of flow effects. For objects in space plasmas, this situation has been summarized by E.C. Whipple in the preceding paper.

When magnetic-field effects are introduced, the problem becomes notoriously intractable. As one would expect, available treatments of it generally involve extreme simplifications. For space applications, the collisionless approximation seems not extreme but instead inevitable. However, we shall see that even in cases of large mean-free-paths, magnetic fields can cause collisional effects to become important.

In spite of this, collisionless theories form the most important category of available theories, and also must be understood before departures from them can be usefully analyzed. Accordingly, a review of collisionless, steady-state theories (Section 2) forms the next part of this presentation. It seems inevitable also to make a further division of such theories, into ones for the zero-space-charge,

or large-Debye-length, limit (one would expect these to be the simplest), and those for finite Debye length. However, even this division is complicated by magnetic-field effects. It turns out that a strictly collisionless theory cannot be exact in cases of finite Debye length, because the disturbance of electric potential produced by the object then extends infinitely far along the magnetic-field direction. However, this conclusion is modified radically by even a small amount of relative plasma drift motion. This situation is discussed in more detail in Sections 3 and 7. Our review includes the work of Sanmartin (1970), who has himself given an extensive review of older theories. A review of probe use in fusion plasmas has been given by Stangeby (1989).

It has often been asked whether any steady-state theory can give a correct prediction, in view of the tendency of fluctuations, or "plasma turbulence", to carry charge across magnetic field lines in magnetic-confinement fusion experiments. Measured return currents in electron-beam-emission experiments in space have frequently been in excess of predicted values from steady-state theory, and such observations have often been cited in support of this view. An alternative explanation, involving energization of ambient electrons by an interaction with the beam, is supported by results of the CHARGE-2 (Myers *et al*, 1989) and SPEAR I (Katz *et al*, 1989) rocket experiments. We discuss this question in Section 4.

Collisional ionization may cause important increases in current collection beyond those predicted by steady-state collisionless theory. The presence of a magnetic field greatly increases phase-space volumes available to particles on "trapped" orbits near the probe, and the long lifetimes of trapped particles in these regions greatly increase opportunities for collisional ionization to occur. The observation of "toroidal glow" regions around spherical probes in low-pressure laboratory magnetoplasmas (W.J. Raitt and A. Konradi, private communication, 1987; Antoniades and Greaves, paper appearing later in these Proceedings) lends support to this idea. Ionization may produce "explosive" growth of the probe's sheath (Lai *et al*, 1985; Cooke and Katz, 1988). Independently of collisional ionization, the existence of trapped orbits also increases the opportunity for current collection to be increased by particle scattering, both collisional and turbulent. We discuss collisional-ionization and collisional-scattering effects in more detail in Section 5.

Enhanced current collection by a probe at large attractive potentials requires increased transport of particles across magnetic-field lines, and this phenomenon is often called "breakdown of magnetic insulation". A brief discussion of some aspects of this phenomenon appears in Section 6.

If the probe is a large object compared with the ambient Debye length, and is moving rapidly compared with the ion thermal speed as in the proposed Tethered Satellite Experiment, a variety of complicated phenomena can occur near it. This situation has been studied by Thompson (1985). A discussion of it appears in Section 7. Unexpectedly, this discussion leads to an inference that even the small relative drift velocities characteristic of rocket experiments can modify radically the processes governing collection of electrons, and can "revalidate" collisionless theories of such collection. A separate issue is the enhancement of current collection by the use of a "plasma contactor" (4 papers, by Hastings, Wilbur and Williams, Katz and Davis, and Cooke, respectively, which appear later in these Proceedings).

Some concluding remarks appear in Section 8.

Much of our discussion in this paper is directed toward current collection at large positive electrode voltages. Interest in predicting such collection has recently increased because of applications to the design of high-voltage power systems for use in space and also because of large induced voltages expected in the Shuttle Electrodynamic Tether experiment.

2. COLLISIONLESS STEADY-STATE THEORIES

In this Section, we consider a spherical probe in a collisionless plasma containing a uniform magnetic field **B**. We give brief summaries of the treatments of Parker and Murphy (1967) and Rubinstein and Laframboise (1982, 1983) and of new results by one of us (L.J.S.). We also summarize results of an analogous treatment which has been done for an infinite cylindrical probe inclined at an arbitrary angle to **B**, by Laframboise and Rubinstein (1976) and Rubinstein and Laframboise (1978). For the spherical-probe case, we choose cylindrical coordinates (r, θ, z) centred on the probe, with the z axis aligned with **B**. In the presence of **B**, our situation no longer has spherical symmetry, and this makes our task much more difficult. However, it still has rotational symmetry about the direction of **B**, and therefore the electric potential ϕ will be independent of θ. In this situation, there are two constants of collisionless particle motion, the total energy E, given by:

$$E = \frac{1}{2}m\left(\dot{r}^2 + r^2\dot{\theta}^2 + \dot{z}^2\right) + q\phi(r, z) \tag{1}$$

and the canonical angular momentum component J about the z axis, given by

$$J = mr^2\dot{\theta} + \frac{1}{2}qBr^2 = mr^2\left(\dot{\theta} + \frac{1}{2}\omega\right) \tag{2}$$

where m and q are particle mass and charge, and $\omega = qB/m$ is the particle's gyrofrequency. We also define the absolute gyrofrequency $\omega_c = |\omega| = eB/m$, where e is the magnitude of unit electronic charge.

We eliminate $\dot{\theta}$ from these two equations, and obtain:

$$E = \frac{1}{2}m\left(\dot{r}^2 + \dot{z}^2\right) + q\phi(r, z) + \frac{m}{2}\left[\frac{J}{mr} - \frac{\omega r}{2}\right]^2 \tag{3}$$

The first term on the right of (3) is the kinetic energy of particle motion in the (r, z) plane. The remaining two terms are then the "effective potential"

$$U(r, z) \equiv q\phi(r, z) + \frac{m}{2}\left[\frac{J}{mr} - \frac{\omega r}{2}\right]^2 \tag{4}$$

for particle motion in the same plane. Since the kinetic energy must be nonnegative, it follows that a particle having a particular E and J will be confined to those regions of the (r, z) plane for which $E \geq U(r, z)$, i.e., inside the particle's "magnetic bottle". Some examples of the general appearance of magnetic bottles are shown in Fig. 1.

Some properties of magnetic bottles follow readily from inspection of Eq. (3); see also Section IV of Rubinstein and Laframboise (1982). These are as follows:

(1) Magnetic bottles have rotational symmetry about the z axis, i.e. their boundaries are independent of θ.

(2) A particle orbit (having a given E and J) can touch the boundary of its magnetic bottle only if $\dot{r}$ and $\dot{z}$ are both zero at the same point on the orbit. Since this is very unlikely, particle orbits generally do not do so.

15

(3) We define a radius r_o by the relation:

$$J = \frac{1}{2}m\omega r_o^2 \qquad (5)$$

(if $\omega > 0$). In Eq. (4), the last term in $U(r,z)$ will then vanish at $r = r_o$, and is positive for $r \neq r_o$, increasing without limit as $r \to 0$ (unless $J = 0$) or as $r \to \infty$. Therefore, particles for which $J \neq 0$ are prevented from reaching the z axis.

(4) For $\omega > 0$, particle orbits for which $J < 0$ encircle the z axis once per gyration; orbits for which $J > 0$ do not.

(5) A nonencircling orbit having energy E and canonical angular momentum J will have the same projection in the (r,z) plane, and also the same magnetic bottle, as those of an encircling orbit having the corresponding values $E + \omega J = E + \frac{1}{2}m\omega^2 r_o^2$ and $-J$. In a strong magnetic field, an encircling orbit will have a much larger energy and also a much larger gyroradius than the corresponding nonencircling orbit, and encircling orbits will then make vanishing contributions to number densities and fluxes.

We now present a derivation of the Parker and Murphy (1967) canonical upper-bound current. Besides the assumption of collisionless, steady-state conditions, their work contained two additional ones. They assumed that any particle whose magnetic bottle intersects the probe is itself collected, and they ignored the effect of a particle's thermal motion at infinity on the question of whether such an intersection exists for that particle. The first assumption results in their current expression being an upper bound on the corresponding exact value. The second assumption amounts to taking the limit $E \to 0$ in Eq. (3). We shall see that this approximation does not lead to an upper bound, so actual currents can exceed the Parker and Murphy (1967) values. When this approximation is made, particles having the largest J for which collection occurs then have a magnetic bottle similar in appearance to that shown as (a) in Fig. 1, but with one important difference: the condition $E \to 0$ means that at large $|z|$, the inner and outer surfaces of the bottle collapse onto the common radius r_o. To find the value of r_o, we make the further substitutions $\dot{r} = 0$, $\dot{\theta} = 0$, $r = r_p$, and $\phi = \phi_p$ in Eq. (3), where ϕ_p is the probe's potential relative to space, r_p is its radius, and $q\phi_p < 0$ for an attractive probe potential for the particle species considered. We then substitute for J using Eq. (5). We obtain:

$$\left(\frac{r_o}{r_p}\right)^2 = 1 \pm \left(\frac{8|q\phi_p|}{m\omega^2 r_p^2}\right)^{\frac{1}{2}} \qquad (6)$$

The positive sign corresponds to tangency of the bottle's inner surface with the probe, as shown in Fig. 1a.

We now note that with Parker and Murphy's approximations, the collected current is equal to the product of the random thermal particle flux with the combined area $2\pi r_o^2$ of the two disks of radius r_o, located at $z = \pm\infty$, through which all collected particles of charge q must pass.

In terms of the random current $I_R = 4\pi r_p^2 q n_\infty (kT/2\pi m)^{\frac{1}{2}}$, and using Eq. (6), we now obtain:

$$i \equiv \frac{I}{I_R} = \frac{1}{2} + \frac{1}{2}\left(\frac{8|q\phi_p|}{m\omega^2\, r_p^2}\right)^{\frac{1}{2}} \qquad (7)$$

where k is Boltzmann's constant, and T and n_∞ are the temperature and ambient number density of the attracted particles. Apart from notation, this is the same as Eq. (13) of Parker and Murphy (1967).

If effects of thermal motion are included, then Eq. (7) is no longer an upper bound on the (collisionless, steady-state) probe current, although we shall see that it remains a good approximate upper bound for large potentials and large magnetic fields. Calculation of the canonical upper bound including thermal-motion effects is much more cumbersome. It has been done by Rubinstein and Laframboise (1982). Here we give only their result, which is in analytic form, as follows:

$$i = i_1 + i_2 \tag{8}$$

where i_1 and i_2 are the (normalized) currents due to nonencircling and encircling particles, respectively, given by:

$$i_1 = \frac{\sqrt{\pi}}{2\sigma}\left(\frac{3}{2} - \psi_p\right) erfc\left(\sqrt{\psi_p}\right) exp\left(\psi_p\right) + \frac{3}{2}\frac{\sqrt{\psi_p}}{\sigma} + \frac{1}{2} \tag{9}$$

$$i_2 = F_1\left(1 + 2\frac{\sqrt{\psi_p}}{\sigma}\right) + F_2\left(1 + 2\frac{\sqrt{\psi_p}}{\sigma}\right) + \frac{1}{2\sigma^2}$$

$$F_1(u) = -\frac{1}{4}\left(\sigma^2 u^2 + 2u + \frac{2}{\sigma^2}\right) exp\left(-\sigma^2 u\right)$$

$$F_2(u) = \frac{\sqrt{\pi}}{4}\left[2\sigma + \frac{1}{\sigma}\left(3 - 2\psi_p\right)\right] erfc\left[\left(\sigma^2 u + \psi_p\right)^{\frac{1}{2}}\right] exp\left(\psi_p\right) \tag{10}$$

$$+ \frac{1}{2}\left\{\left[\frac{3}{\sigma} + 2\sigma\left(1 + u\right)\right]\left(\sigma^2 u + \psi_p\right)^{\frac{1}{2}} - 3 - 2\psi_p\right.$$

$$\left. - \sigma^2\left(3u + \frac{1}{2}\right)\right\} exp\left(-\sigma^2 u\right)$$

$$\sigma = \frac{1}{2}\sqrt{\pi}\beta$$

where $\beta = r_p/\bar{a} = r_p|\omega|(2m/\pi kT)^{\frac{1}{2}}$ is the ratio of probe radius to mean attracted-particle gyroradius, and $\psi_p = -q\phi_p/kT \geq 0$ is dimensionless probe potential. Rubinstein and Laframboise (1982) also obtained a corresponding analytic result for repelling probe potentials $\psi_p < 0$, given by their Eqs. (30), (36), and (37), and plotted in their Fig. 10. In contrast with the usual exponential variation of collected current at these potentials, their result shows a "rounding of the knee" of the probe's current-voltage characteristic at small negative ψ_p. In the limit of large attractive potentials $\psi_p \gg 1$, Eqs. (8) − (10) reduce to:

$$i = \frac{1}{2} + \frac{\sqrt{\psi_p}}{\sigma} + \frac{1}{2\sigma^2} \tag{11}$$

The first two terms of this are the same as the Parker and Murphy (1967) result. The last term is a contribution from encircling orbits, which vanishes in the limit of strong magnetic fields: $\beta \to \infty$. A comparison of the Parker-Murphy (1967) canonical upper bound with results of Rubinstein and Laframboise (1982) for attracted-species currents is shown in Fig. 2. The increasing curves in Fig. 2 show least upper-bound currents. The portions of these curves to the right of the "kinks" (discontinuities of slope) are the canonical upper bounds given by Eqs. (8) − (10). The portions to the left of the kinks are "helical" upper bounds also calculated by them, and based on an

assumption that particle orbits are helices near the probe. The decreasing curves are adiabatic-limit (effectively lower-bound) currents also calculated by them, also assuming helical orbits near the probe, but assuming a "one-dimensional" rather than "three-dimensional" velocity-space cutoff. For a probe at space potential, $\psi_p = 0$, the upper-bound and adiabatic-limit currents coincide, and are the same as those given in Fig. 17 of Whipple (1965). For any given value of β, we see that the upper-bound and lower-bound curves separate rapidly as ψ_p increases. This is clearly an unsatisfactory situation, but it appears to represent the best that can be done without resorting to the expense of numerical orbit integration. We present results of such a calculation below.

As mentioned above, the adiabatic-limit currents decrease as ψ_p increases. This "negative-resistance" behavior results from the fact that in the adiabatic limit, the kinetic-energy gain of incoming particles goes entirely into increased speed parallel to **B**. This increases the pitch of their orbits. Some orbits whose pitch becomes greater than roughly the probe diameter can now bypass the probe, and current collection will be decreased. When ψ_p is small, we also expect the actual currents to approach the adiabatic-limit currents, since the adiabatic-limit condition is that changes in the probe sheath electric field are small over an average particle gyroradius. We further expect that as ψ_p becomes more positive, adiabatic-limit conditions will break down, and collected currents will then rise toward the upper-bound values.

We therefore expect the current-voltage characteristics to be "N-shaped". Such behavior was predicted qualitatively by Laframboise and Rubinstein (1976) and Rubinstein and Laframboise (1982), and more recently seen in data from spherical electrostatic probes on the University of Iowa Plasma Diagnostics Package flown on several Shuttle flights (G.B. Murphy, private communication, 1983). We present later in this Section a quantitative prediction of such characteristics.

Figure 3 shows the same comparison of the Parker and Murphy (1967) and Rubinstein and Laframboise (1982) upper-bound currents over a larger range of attractive probe potentials. It is evident from this Figure, and also from Eq. (11), that these bounds do not coalesce at large potentials, but only for large magnetic fields.

Corresponding upper and lower bounds on current have been calculated for an infinite-cylindrical probe inclined at an arbitrary angle to **B** by Laframboise and Rubinstein (1976) and Rubinstein and Laframboise (1978), and for spheroids and finite cylinders, including disks, whose axis of symmetry is aligned with **B**, by Rubinstein and Laframboise (1983). In all cases, their helical upper-bound and adiabatic-limit currents depend on all aspects of probe shape, whereas their canonical upper-bound currents depend only on the probe cross-section perpendicular to **B**. We reproduce here only their result for the canonical upper-bound current to an infinite cylindrical probe. For the cylindrical case only, we redefine I and I_R to be the current and the random current $2\pi r_p q n_\infty (kT/2\pi m)^{\frac{1}{2}}$, respectively, both per unit probe length. For the attracted particles ($\psi_p \geq 0$), their result [Rubinstein and Laframboise, 1978, Eqs. (10) and (11)] is:

$$i = \frac{2}{\pi}\sin\theta + \frac{1}{\pi^{3/2}\beta}\left[\left(3 - 2\psi_p\right)\sqrt{\pi}\ erfc\left(\sqrt{\psi_p}\right)exp\left(\psi_p\right) + 6\sqrt{\psi_p}\ \right] \tag{12}$$

where θ is the angle between the probe axis and the direction of **B**. For large ψ_p:

$$i \rightarrow \frac{2}{\pi}\sin\theta + \frac{4}{\pi^{3/2}}\frac{\sqrt{\psi_p}}{\beta} = \frac{2}{\pi}\sin\theta + \left(\frac{8|q\phi_p|}{\pi^2 m\omega^2 r_p^2}\right)^{\frac{1}{2}} \tag{13}$$

A corresponding result for repelling probe potentials $\psi_p < 0$ is given by their Eq. (13). The most remarkable feature of our Eq. (13) is that it gives the same one-half-power dependence of probe

current on probe potential as in the spherical case [Eqs. (7) and (11)], in spite of the difference in probe shape. As in the spherical case, the canonical upper bound may not be the least upper bound, especially at small β and ψ_p; see Figs. 2 and 3 of Rubinstein and Laframboise (1978). Equations (12) and (13) should be useful for estimation of currents collected by tether wires in space.

All of this leaves unanswered so far the question of how nearly the actual current collection approaches these upper-bound values. For cylindrical probes, experimental data presented in Fig. 4 of Szuszczewicz and Takacs (1979) provide a partial answer to this question. They found that adiabatic conditions are easily violated in the cylindrical configuration. For spherical probes in the limit of large Debye length (Laplace-potential limit), we present results from an exact numerical calculation of probe currents by one of us (L.J. Sonmor, Ph.D. thesis, in preparation). This calculation is "exact" in the sense that in the limit of zero discretization and roundoff errors, it would produce results corresponding exactly to the physical assumptions made.

In the Laplace-potential limit, an important computational advantage can be gained by scaling the collisionless charged-particle orbits. These obey the equation of motion $m\ddot{\mathbf{r}} = q\,(\mathbf{E} + \dot{\mathbf{r}} \times \mathbf{B})$. We introduce the scaled position vector $\tilde{\mathbf{r}} = \mathbf{r}/(|m\phi_p r_p/qB^2|)^{1/3}$ and time $\tau = (qB/m)t$. This equation then reduces to:

$$\frac{d^2\tilde{\mathbf{r}}}{d\tau^2} = \pm \frac{\mathbf{i}_r\tilde{r} + \mathbf{i}_z\tilde{z}}{(\tilde{r}^2 + \tilde{z}^2)^{3/2}} + \frac{d\tilde{\mathbf{r}}}{d\tau} \times \mathbf{i}_z \tag{14}$$

which contains no free parameters. The calculation method then involves integration of (14) for various scaled initial positions $\tilde{\mathbf{r}}$ and velocities $d\tilde{\mathbf{r}}/d\tau$ on a plane $\tilde{z}$ = constant located sufficiently far from the origin of coordinates. This yields a data base of distances of closest approach to the origin. The appropriate integration over this data base then yields the current-voltage characteristics (i vs ψ_p for various β). Separate data bases must be created for attractive and repulsive probe potentials. To obtain values of i having a relative accuracy of 1% or better required the integration of about two million such orbits, and this consumed about 25 hours of CPU time on the University of Toronto CRAY X-MP computer.

Results from this calculation are shown in Figures 4-7. Figures 4(a) - (d) show representative particle orbits, together with their corresponding magnetic-bottle boundaries. The orbits shown all have positive total energies ($E > 0$) so they all originate at $z = \pm\infty$. As we mentioned following Eq. (4), such orbits generally do not touch their bottle boundaries, but they evidently come very close to them near points of reversal of z velocity, because $|\dot{r}|$ and $|\dot{z}|$ can be simultaneously very small near such points. Our earlier discussion implies that actual currents will equal canonical-upper-bound values [Eqs. (8) - (10)] if every orbit reaches the point closest to the origin on its bottle boundary, but that in general, orbits do not do so. Comparison of Figures 4(b) - (d) shows that the nearness of an orbit's approach to this point can be very sensitive to its initial phase. Figures 4(a) - (d) also show significant violation of the adiabatic-limit approximation, including, in (b) - (d), reversals of z-velocity.

Figures 5 and 6 show attracted-particle current-voltage characteristics for smaller and larger ranges of attractive probe potential, respectively, and for two different values of β. Also shown are the Rubinstein and Laframboise (1982) canonical upper bound [Eqs. (8) - (10)], and, in Figs. 5(a) and (b), their helical upper bound and adiabatic limit. Features visible in Figs. 5(a) and (b) include, as predicted above, a negative-resistance region in the attracted-particle current-voltage characteristic. When $\beta = 3$, this region extends over a larger range of probe potentials than when $\beta = 1$.

In this region, the slope of the exact characteristic appears to be less negative than that of the adiabatic-limit curve everywhere, even at small potentials. One can identify three possible reasons for this. One of these is that the mechanism causing this bahavior, namely that some orbits miss the probe because they are "stretched", *i.e.*, their pitch is increased near it, does not operate as effectively for the real orbits as for the helical ones assumed in the adiabatic-limit calculation. Another is that nonadiabatic effects also cause some particle gyroradii to increase (Fig. 4), allowing more particles to be collected. A third possible reason is radial drift motions caused by electric-field inhomogeneities (Fig. 4a). A current-collection theory based on such drift motions was developed by Parker and Murphy (1967, Fig. 2 and Table 1).

Figures 5 and 6 appear to leave unresolved the important question of whether the exact currents approach the canonical upper-bound values at large attractive potentials or remain substantially below them. This question is examined directly in Fig. 7, but the outcome is still not clear. What is clear from Fig. 7 is that even if the actual currents approach the canonical upper-bound currents at large potentials, the approach is so slow as to be irrelevant to most practical purposes. It is noteworthy that at the largest probe potential shown in Fig. 7, *i.e.* $\psi_p = 500$, the Parker-Murphy (1967) canonical-bound values are much closer to the Rubinstein-Laframboise (1982) values than the exact currents are, so the latter currents also remain substantially below the corresponding Parker-Murphy values. Some evidence of the level of numerical errors in these "exact" results also appears in Figs. 6(a) and 6(b).

An important limitation of the exact results shown in Figs. 4-7 is that they apply only in the Large-Debye-length limit. As the Debye length is decreased, space-charge effects influence more and more strongly the potential disturbance around the probe. As a result, this potential becomes progressively more "short-range", with increased electric fields in the sheath region near the probe, and decreased fields in the presheath region farther away (see below, however). M.J. Mandell (private communication, 1989) has suggested that in this situation, the current collection may increase above the values shown in Figs. 5-7 toward the canonical-upper-bound values, because adiabatic-limit conditions now are more strongly violated near the probe, and this permits incoming particles to acquire larger gyroradii, so that more of them are collected. This is in contrast with the nonmagnetic situation, in which attracted-species current collection decreases with decreasing Debye length; see, for example, the preceding paper by E.C. Whipple.

Figure 7 contains a feature which may illuminate this question. This Figure shows a "crossover" of the current-voltage curves for various values of β as the probe voltage ψ_p increases, with the currents for the largest β values becoming the closest ones to the upper-bound currents at the largest ψ_p values shown. If one considers the magnetic bottles which correspond to the attracted-particle energies making the most important current contributions at large ψ_p, then among these bottles, those which correspond to the largest β values will have the least relative widening (Figs. 1 and 4) near $z = 0$. Figure 7 therefore implies a tendency for bottles with the least widening to be the "most filled" by the orbits confined inside them. If this tendency carries through to situations in which space-charge effects are important, it will tend to counteract the mechanism described in the preceding paragraph, and the attracted-species current may then decrease rather than increase with decreasing Debye length as in the nonmagnetic case. Another mechanism which may act in the same direction is the tendency of magnetic bottles to form "bulges" or even disjoint "bubbles" as a result of space-charge effects on the probe sheath potential distribution (Section 5).

20

3. COMBINED EFFECTS OF SPACE-CHARGE AND COLLISIONS

In some presheath locations, a decrease in Debye length will produce an increased rather than decreased electric field. To see why, we consider the depletion of particles at large distances from a spherical probe, caused by the probe's current collection. If $B = 0$, this depletion occurs equally in all directions for both ions and electrons, and therefore results in a spherically-symmetric distribution of net space charge and therefore of potential. If $B \neq 0$, it occurs predominantly along and adjacent to the probe's "magnetic shadow". In other words, we expect that at large $|z|$, both the ion and electron density disturbances (in the collisionless limit) will become functions only of the cylindrical radius r. In contrast with the nonmagnetic case, however, these disturbances will have different dependences on r for the ions and electrons, because the much smaller average gyroradius of the electrons will cause the electron depletion to be confined much more closely to the magnetic shadow itself, whereas the ion depletion will be more widespread (Fig. 8). If the Debye length is finite, the resulting charge imbalances will produce a potential disturbance which will also depend only on r at large $|z|$. Unless the probe potential is very negative, this disturbance will be positive in sign (Sanmartin, 1970). In the absence of collisions (and assuming steady-state conditions), no mechanism exists to cause the charge-density disturbances to decay with increasing $|z|$, and the resulting potential disturbance must therefore also extend to infinity in both directions along the probe's magnetic shadow. This further implies that if the charged-particle mean-free-paths are finite, no matter how large they are, collisions will ultimately repopulate the depleted regions as $|z| \to \infty$. Some of these collisionally-redirected particles will travel toward the probe. In doing so, they will produce effects on both the space-charge density near it and on current collection by it. Some of the same particles will have negative values of the total energy E defined in Eq. (1); if the potential disturbance is positive in sign, this can happen only for electrons. These particles cannot escape from the probe's potential disturbance unless it extends to infinity or they undergo another collision; otherwise the z component of their velocity, if initially directed away from the probe, must eventually reverse. The electron current reaching the probe will therefore include a contribution due to electrons which have negative total energies. In contrast with the situation for $B = 0$, this contribution will persist rather than vanish in the limit of large mean-free-paths; increasing the mean-free-path will result merely in a corresponding increase of the scale of distances over which collisions provide this contribution.

We therefore conclude that a collisionless, finite-Debye-length theory cannot be formulated for a probe in a magnetoplasma, unless some approximation is made (discussions with H.A. Cohen, unpublished). On the other hand, effects of this may be negligible in at least some real situations. For example, the calculations reported by Katz *et al* (1989), which were done in support of the SPEAR I electrostatic probe measurements using the NASCAP/LEO and POLAR simulation programs, gave good agreement (within about 4% in the case of the more-accurate POLAR calculations) with these measurements (see their Fig. 10), and these were collisionless calculations. The NASCAP/LEO calculations used analytic approximations for space-charge densities in the sheaths around the SPEAR I probes and rocket body, whereas POLAR calculated these densities by tracking particle orbits inward from sheath edges. It is noteworthy also that all the theory which we have discussed so far has been for a nondrifting ambient plasma. In Section 7, we discuss a description by Thompson (1985) of the disturbed region around a high-voltage orbiting object. Thompson's description implies that a drift transverse to B, even at much less than orbital speed, may change fundamentally the structure of this disturbed region, and a completely collisionless calculation of collected current then may still be applicable. We discuss this question in more detail in Section 7. Here we confine our discussion to nondrifting situations.

The most thorough available treatment of the combined effects of collisions and space-charge on probe current is that of Sanmartin (1970), who performed an asymptotic analysis on this problem, using ion and electron collision models based on cumulative small-angle scattering by multiple Coulomb encounters. In his treatment, electron collection by the probe is limited by the fluxes of electrons which are supplied by collisions to the above-mentioned two regions (one for $z > 0$ and one for $z < 0$) of positive potentials in the probe's magnetic shadow. To be collected, these electrons must also cross a potential barrier which exists between each of these regions and the probe when the probe potential is close enough to space potential. This barrier exists because at such probe potentials, each region is more positive than at either the probe or infinity, i.e., there is an "overshoot" in the potential distribution as a function of $|z|$ in each region (Fig. 9). The most important effect of this situation on the probe current near space potential is to decrease the electron collection, thereby "rounding the knee" of the probe's current-voltage characteristics as computed by Sanmartin. His results for the electron-current characteristics are reproduced in Fig. 10. Sanmartin's treatment assumes that the ion-to-electron temperature ratio is close to unity, the electron average gyroradius $\bar{a}$ and the Debye length λ_D are both $<< r_p$, and $r_p \lesssim$ both the mean free path for multiple small-angle Coulomb collisions and the ion average gyroradius. In his analysis, the magnetic shadow region on each side of the probe is divided into: an outer layer which extends to infinity, is quasineutral and collision-dominated, and in which the potential rises to a maximum value as one approaches the probe; an intermediate layer, also quasineutral, across which the potential is uniform and whose thickness is of the order of the local electron mean free path; and an inner layer which is collisionless and in which the potential decreases steeply to its value on the probe. Sanmartin's approximations include a point-to-point matching of the particle fluxes as a function of r across the intermediate layer. For electrons, this is done by equating his Eqs. (44) and (65) for these fluxes. The result is to exclude the possibility of an attraction-region increase in current collection due to effects of particle orbital motions, so his attraction-region currents saturate at $i = \frac{1}{2}$ as $\psi_p \to \infty$, in contradiction with the results discussed in Section 2. His theory in its present form therefore is useful primarily for probe potentials close to space potential when $r_p >> \lambda_D$ and the magnetic field is large enough that $\beta = r_p/\bar{a} >> 1$ (See, however, the last paragraph of Section 4). For a probe at space potential, $\psi_p = 0$, the currents predicted by him (Fig. 10) are much lower than the collisionless currents given by Fig. 17 of Whipple (1965) for the case $r_p << \lambda_D$. At present, there is no theory available for probes in magnetoplasmas which includes effects of particle orbital motions together with collisional and space-charge effects, and we have seen (Section 2) that at larger probe potentials, orbital-motion effects become increasingly important.

4. EFFECTS OF PLASMA TURBULENCE

A persistent and widespread suspicion has been that when probe potential is sufficiently positive, spontaneous fluctuations or "plasma turbulence", driven by the large electron-density gradients which then exist near the edges of the probe's magnetic shadow, will transport charged particles transversely to **B** and produce probe currents much larger than those predicted by the steady-state theories described in Sections 2 and 3. The existence of probe-induced spontaneous fluctuations, for probes having a sufficiently large positive bias, is well-established by laboratory observations (Balmain, 1972; Urrutia and Stenzel, 1986; Stenzel, 1988). Spontaneous density fluctuations of up to a few percent amplitude have also been observed in the disturbed region around the Shuttle Orbiter (Murphy et al, 1986). What is less clear is whether such fluctuations can increase substantially the time-averaged currents collected by probes.

For a long time, only one theoretical treatment, due to Linson (1969), has been available which includes predictions of plasma turbulence effects on current collection by a probe. An alternative formulation by P.J. Palmadesso appears later in these Proceedings.

Linson's (1969) treatment is semi-empirical because it depends on a parameter whose value is inferred from experimental data rather than predicted. Linson suggests that the unneutralized electron population in the sheath region around a probe having a large positive bias may be subject to a gyroresonant instability whose onset depends on a sufficiently large value of the parameter:

$$Q = \omega_e^2 / \omega_c^2 \tag{15}$$

where $\omega_e = (n_e e^2 / m_e \epsilon_o)^{\frac{1}{2}}$ is the electron plasma frequency, $\omega_c = eB/m_e$ is the electron gyrofrequency, m_e and n_e are electron mass and number density, and ϵ_o is the permittivity of space. Linson cites evidence that the onset of this instability occurs when Q is close to or somewhat smaller than 1; ionospheric values of Q are generally greater than 1. Linson then assumes that the resulting turbulent diffusion produces a region of uniform electron density around the probe (Fig. 11), that this region is greatly extended in the z direction, and that electric fields parallel to z are small compared to those perpendicular to z. Assuming also that ions are completely excluded from this region then permits him to write a cylindrically-symmetric Poisson equation:

$$\frac{1}{r}\frac{d}{dr}\left(r\frac{d\phi}{dr}\right) = \frac{en_e}{\epsilon_o} \tag{16}$$

for potentials within it. He solves this equation subject to the boundary conditions:

$$\phi = \phi_p \text{ when } r = r_p \tag{17}$$

$$\phi = 0, \frac{d\phi}{dr} = 0 \text{ when } r = r_s \tag{18}$$

Equation (16) is of only second order, so with three boundary conditions given in Eqs. (17) and (18), this system of equations is overdetermined. Solving it therefore also provides a value for the sheath radius r_s. We obtain:

$$\phi_p = \frac{1}{2}Q\phi^* \left\{ \left(\frac{r_s}{r_p}\right)^2 \left[ln\left(\frac{r_s}{r_p}\right)^2 - 1 \right] + 1 \right\} \tag{19}$$

where $\phi^* = \frac{1}{2}m_e\omega_c^2 r_p^2 /e$. This result is Linson's Eq. (13). It provides an implicit relation for r_s as a function of the probe potential ϕ_p. Linson then proposes, as an upper bound on probe current, the random current incident on both ends of a flux tube of radius r_s. In terms of the random current I_R defined just prior to Eq. (6), Linson's upper-bound current is now given by:

$$i = I/I_R = \frac{1}{2}\left(r_s/r_p\right)^2 \tag{20}$$

Figure 12, which is a reproduction of Linson's Figure 3, shows a comparison of the currents given by Linson's treatment for $Q = \frac{1}{4}$ and 1 with those given by the result of Parker and Murphy (1967) [our Eq. (7)] and by the nonmagnetic, spherically-symmetric, space-charge-limited theory of Langmuir and Blodgett (1924). This Figure suggests that turbulent transport produces a major increase in the probe's electron collection, perhaps to values close to the nonmagnetic ones.

23

Experimental evidence for this contention has been ambiguous until recently. This is in spite of the launching, since 1969, of no fewer than 25 separate rocket and satellite experiments which included measurements of the potential acquired by surfaces of the vehicle when an electron beam was emitted from it. Reviews of these experiments have been given by Winckler (1980), Linson (1982), Szuszczewicz (1985), and Maehlum (1988). During the same period, space experiments have also been performed which involved either the emission of ion beams, with measurements of the resulting vehicle surface potentials, or the application of a differential bias which caused one part of the vehicle to acquire a large negative potential relative to space, with the resulting ion collection current measured. In such cases, magnetic-field effects on ion collection are relatively small because of the relatively large average gyroradii of ions. Of greater importance in these cases are effects of relative ion drift motion. Exact collisionless theory for ion collection in the presence of ion drift is relatively incomplete. A review of available approximate theories for this situation has been given by Godard and Laframboise (1983). Substantial disagreement exists between these theories and experimental results (Makita and Kuriki 1977, 1978) but the approximations in the theories are severe enough that this does not constitute evidence that the collisionless, steady-state model is invalid for ion collection. In contrast with this, the electron current-voltage observations generally imply currents exceeding the Parker and Murphy (1967) values. The amount of excess current appears to increase with ambient electron density. Popadopoulos and Szuszczewicz (1986) have proposed that a collective interaction between the beam and the ambient plasma may energize some of the ambient electrons, and these then provide a greatly increased return current to the vehicle because of their much larger velocities.

This hypothesis is supported by the results of the recent CHARGE-2 (Myers *et al*, 1989) and SPEAR I (Katz *et al*, 1989) rocket experiments. In the CHARGE-2 experiment, the payload was separated into two sections joined by an insulated conducting tether. One of the sections carried a 1 *keV* electron gun. The sections were separated by up to 426*m* across the geomagnetic field. Return current collection was observed for positive potentials up to 1 *kV* on both sections. In all measurements, return currents to the section carrying the gun exceeded Parker-Murphy (1967) values, while those to the other section agreed well with these values. In the SPEAR I experiment, no beam was emitted. SPEAR I carried two spherical electrostatic probes of radius 10*cm*, separated from each other by 1*m* and from the rocket body by 3*m*. Positive voltages up to 45.3*kV* were applied to one of the two spheres. In the results presented by Katz *et al* (1989), the other sphere was grounded to the rocket body. Also grounded to the rocket body was a stem which supported both probes and was separated from them by resistive bushings of length 1*m*. Katz *et al* (1989) calculated that when a 46*kV* bias was applied to one sphere, the rocket body and the other sphere floated at $-8.3kV$, and the biased sphere then floated at 37.7*kV*. The measured current-voltage curve gives a current of 52 *mA* at this voltage. This is about twice the Parker-Murphy (1967) value [Eq. (7)] for these conditions, but the calculations of Katz *et al* (1989) indicate that this discrepancy results from the breaking of canonical angular momentum conservation [Eq. (2)] by the strong asymmetry of the sheath around the probe; this asymmetry in turn is produced by the presence of the oppositely-biased large rocket body and other probe (I. Katz, private communication, 1989). The results of this experiment therefore can be interpreted as providing further support for the validity of the canonical upper bound on current collection [In these experiments, the correction term $\frac{1}{2}/\sigma^2$ in Eq. (11) was negligible, so the canonical upper bound was essentially equal to the Parker and Murphy (1967) upper bound given by Eq. (7)]. This in turn indicates an absence of significant turbulent-transport effects on such currents in the absence of beam-induced disturbances, contrary to the hypothesis advanced at the beginning of this Section.

However, Palmadesso (paper appearing later in these Proceedings) has pointed out that one

expects turbulent-transport effects to become important only when the region of large electric fields near the probe extends radially beyond the region in which the probe is readily accessible to particles on the basis of steady-state fields only. For the radii of these two regions, he uses the nonmagnetic spherical sheath solution of Langmuir and Blodgett (1924) and the Parker-Murphy (1967) radius r_o, given by Eq. (6) with a positive sign, respectively. He points out that the Langmuir-Blodgett radius is initially smaller but grows more rapidly as probe potential increases, so one should expect significant turbulent transport effects only for large enough values of probe potential. This appears to indicate that turbulent transport may yet prove to be important at large enough positive voltages, so the indications to the contrary provided by the CHARGE-2 and SPEAR I experiments may not be conclusive.

This apparent absence of turbulent-transport effects in space situations runs counter to widespread expectations, as we noted at the beginning of this Section. An example of such expectations is a discussion by Stangeby (1989, Sec. IIIA) of particle transport across magnetic fields in magnetic-confinement fusion experiments. Stangeby summarizes the evidence for the well-known conclusion that such transport generally agrees with the empirically-obtained Bohm value (Bohm et al, 1949), and is much larger than the "classical" value which forms the basis of the Sanmartin (1970) theory discussed in Sec. 3. However, probe use in fusion plasmas generally involves very different conditions than in space (P.C. Stangeby, private communication, 1990). Because of interpretive difficulties, probes in fusion plasmas are generally operated at voltages below floating potential (Stangeby and McCracken, 1990, Figures 2.4 and 2.5). Ion and electron densities are then nearly equal to each other almost to the probe surface, whereas in the CHARGE-2 and SPEAR I situations, the probes were surrounded by large electron sheaths. This difference presumably affects the turbulent-transport mechanisms involved, but these are understood very poorly, so firm conclusions cannot be drawn.

5. PARTICLE TRAPPING AND THE "TOROIDAL GLOW" REGION

We have seen that imposition of a magnetic field changes fundamentally the characteristic motions of charged particles in the disturbed region around a probe (Sections 2 and 3). An important consequence of this is a qualitative increase in the possibilities for trapping of attracted particles in this region. This in turn creates the possibility of significant increases in probe current because of collisional or turbulent scattering into and out of this region, or collisional ionization of neutrals in it. We examine each of these aspects of this situation separately.

We illustrate in Fig. 13 the region of space in which particle trapping occurs in the presence of a magnetic field. For the attracted-particle species $[q\phi_p < 0]$, this Figure shows the general appearance of "open" magnetic bottles which extend to $z = \pm\infty$ and correspond to $E > 0$, and "closed" ones which correspond to $E < 0$, all drawn for a particular value of J which is chosen such that the bottle for $E = 0$ marginally fails to intersect the probe. Since $\phi = 0$ at infinity, $E > 0$ for all particles coming from the ambient plasma. Therefore, in the absence of collisions, the "trapped-orbit" $(E < 0)$ region of one-particle phase space, corresponding to closed magnetic bottles such as those shown in Fig. 13, must remain unpopulated. However, if a particle is scattered into this region, by either a collision or (possibly) a turbulent scattering event, it will remain there until another such event scatters it out again. If the collision frequency is very small, such a particle is likely to remain there for a very long time. Therefore, even in the limit of small collision frequency, a steady-state particle population will build up in the trapped-orbit region. This population will not be larger than the equilibrium value given by the usual Boltzmann factor, but this bound permits very large attracted-species populations if potentials near the probe are very large. This population will always remain less than the equilibrium value, because particles can also be scattered out of

it into "collection" orbits which intersect the probe. Assuming that the probe is nonemissive, this sets up a net unbalanced flux of particles into it, using the trapped orbits as an intermediary stage (Fig. 14), and therefore detailed balancing cannot occur, and an equilibrium population of these orbits cannot be attained. This unbalanced flux also constitutes an additional current to the probe. So far, the problem of calculating this current is completely unsolved.

In the absence of a magnetic field, approaches to this problem have been made by Wasserstrom *et al* (1965), Chou *et al* (1966), Bienkowski and Chang (1968), Self and Shih (1968), Talbot and Chou (1969), Thornton (1971), Shih and Levi (1971), Parker (1973), Friedland and Kagan (1979), and others, using various approximations. A review of most of this work has been given by Chung *et al* (1975, Section 2.5).

Our depiction in Fig. 14 of the intermediary role of trapped orbits is schematic, and applies whether or not a magnetic field is present, even though the orbits when $\mathbf{B} \neq \mathbf{0}$ will generally be more complicated than those shown. However, one feature of the trapping phenomenon is fundamentally different when $\mathbf{B} \neq \mathbf{0}$. In either the nonmagnetic or magnetic case, the term $q\phi(r,z)$ in Eq. (4) will have a local minimum as a function of z at $z = 0$ for each r, so trapping will occur, *i.e.* the effective potential $U(r,z)$ in Eq. (4) will have a local minimum, if the last term in Eq. (4) has a minimum outside the probe as a function of r for at least some values of J. Inspection of this term shows that in the nonmagnetic case ($\omega = 0$), this term has minima only if $|q\phi(r,z)|$ decreases more slowly as a function of r than an inverse-square potential $\phi = $ const. r^{-2} over at least some range of r values (Mott-Smith and Langmuir, 1926; Bernstein and Rabinowitz, 1959; Laframboise, 1966; Laframboise and Parker, 1973). Accumulation of a trapped-particle population adds space charge of a sign opposite to that on the probe surface, and this causes the sheath potential to steepen, tending to destroy the conditions necessary for trapped orbits to exist, and thereby limiting their population (Laframboise, 1966, Section VIII). However, in the magnetic case, the last term in Eq. (4) always has minima as a function of r. A steepening of the potential therefore can modify the resulting minima of the effective potential $U(r,z)$, but cannot destroy them. We therefore expect trapped-orbit effects to be much more important when significant magnetic fields are present.

We have so far not mentioned what may be the most important consequence of trapped-orbit population. Particles scattered into the trapped-orbit region will be accelerated by large electric fields in this region if the probe potential is large. In the more central regions of the closed magnetic bottle accessible to each particle, it will then have enough kinetic energy to cause collisional ionization of neutrals. If the attracted particles are electrons, this will occur for probe potentials above a few hundred volts. Some of the new charged particles thus produced will be on collection orbits (Fig. 14), and this can produce a substantial increase in probe current. Another consequence of energetic collisions in the trapped-orbit region is light emission. Such emission was first observed as a "toroidal glow" region, in a laboratory experiment by W.J. Raitt and A. Konradi (private communication, 1987). The toroidal-glow phenomenon has since been studied in detail by Antoniades and Greaves (paper appearing later in these Proceedings), who have also observed the above-mentioned increase in probe current. They have observed these phenomena in a test chamber which was large enough to permit a well-developed trapped-orbit region to exist around the probe, but they did not see them in tests done in a smaller chamber. So far, these phenomena have not been observed in space. Antoniades and Greaves discuss in detail the conditions under which one can expect them to occur. One feature of the toroidal-glow region, which may be expected on the basis of Fig. 13, is that it should have "pointed ends" in the $\pm z$ directions, and this feature is evident in photographs of it presented in their paper.

When the magnetic field is sufficiently weak, their results show that the toroidal-glow region disappears and either no discharge or a spherically-symmetric discharge occurs. If the ambient

neutral density is large enough, the establishment of a spherically-symmetric discharge, around a probe at a large positive voltage, involves a process of "explosive sheath ionization", which has been studied by Lai *et al* (1985) and Cooke and Katz (1988). In this process, electrons created by ionization of neutrals in the sheath migrate quickly to the probe, while similarly-created ions accelerate slowly away from it. This results in a net positive contribution to the space charge in the probe sheath. This contribution enlarges the sheath and thereby enlarges the region in which the electrons have been accelerated through a sufficient change of potential to ionize neutrals. This results in more net positive space charge and a consequent runaway sheath expansion.

Magnetic-bottle shapes similar to those shown in Figs. 1, 4, and 13 do not exhaust all possibilities. The dependence of $|\phi(r,z)|$ on r for $z \approx 0$ in a steady-state situation invariably involves a steep decrease toward space potential in the sheath region, followed by a much less rapid decrease in the presheath region beyond the sheath edge. For some values of J, the effective potential $U(r,z)$ for the attracted particle species in Eq. 4 may then have, instead of a single minimum as a function of r for $z = 0$, two minima separated by a maximum. Depending on the value of E, this can cause the corresponding magnetic bottles to have "bulges" or even disjoint "bubble" regions (Fig. 15). In the latter case, particles travelling along collisionless orbits from infinity will be unable to enter these "bubble" regions even though permitted by their values of E and J to exist there. In the case of "bulges", such particles are likely to be partly prevented from entering the bottle regions closest to the probe; a similar effect was discussed in connection with bottle "widening" at the end of Section 2. To some extent, all of these effects will limit access to the probe of attracted-species particles which initially (*i.e.* far from the probe) move along orbits located outside the probe's magnetic shadow. This may possibly invalidate the conjecture, mentioned at the end of Section 2, that space-charge effects on the potential $\phi(r,z)$ may cause the current collection to increase above the Laplace-limit values calculated by Sonmor (see Section 2), toward the canonical-upper-bound values. However, the SPEAR I and CHARGE-2 current-collection values discussed in Sections 3 and 4 appear to show good agreement with the canonical-upper-bound values, so at present there is no clear experimental evidence for a collected-current decrease caused by the formation of "bulges" and the breakup of magnetic bottles into disjoint "bubble" regions. As noted in Section 2, the numerical results of Sonmor support the idea that this may occur. However, a definitive answer to this question will require a more specific investigation of it than any done so far.

6. BREAKDOWN OF MAGNETIC INSULATION

"Magnetic insulation" is the tendency of a magnetic field to inhibit the transport of charged particles across magnetic flux surfaces. In Sections 2-5, we have considered various ways in which magnetic insulation can break down and current collection by a probe can increase as probe voltage becomes more attractive for the particle species considered (most specifically, the electrons). We have examined effects of violation of adiabatic invariance (Section 2), collisions (Sections 3 and 5), self-excited fluctuations (Sections 4 and 5) and particle trapping combined with collisions, fluctuations, or collisional ionization (Section 5). Here we take a different view of the collisionless particle motions treated in Section 2 (discussions with D.L. Cooke, unpublished). We consider specifically the motions of particles in the trapped-orbit or "toroidal glow" region discussed in Section 5. For particles which have a small enough z-component of velocity, one may expect these motions to be well-approximated by a circumferential $\mathbf{E} \times \mathbf{B}$ drift with superposed gyromotion in the plane $z = 0$, together with small oscillations about this plane. However, we now show that this is not necessarily the case.

To show this, we note that the usual analysis for particle motion in uniform crossed $\mathbf{E}$ and $\mathbf{B}$ fields (see, for instance, Tanenbaum, 1967, Section 1.4) yields an $\mathbf{E} \times \mathbf{B}$ drift velocity

$\mathbf{v_d} = (\mathbf{E} \times \mathbf{B})/B^2$. The magnitude of $\mathbf{v_d}$ is E/B. This can easily exceed the speed of light. This happens when $E > Bc$. For $B = 0.3$ Gauss $= 3 \times 10^{-5}T$, corresponding to the low-latitude ionosphere, and $c = 3 \times 10^8 m/sec$, this inequality becomes $E > 9000V/m$. The SPEAR I probes had radius $r_p = 10cm$. Ignoring space-charge effects gives a surface electric field E_r on these probes given by $E_r = -(d\phi/dr)_p = \phi_p/r_p$. The above-mentioned inequality is then fulfilled when the probe potential $\phi_p > 900V$. Since space-charge effects can be expected to increase electric fields near a probe, this inequality would have been fulfilled at even lower probe voltages in the SPEAR I experiment. Since drift velocities greater than the speed of light are impossible, something is clearly wrong with this analysis.

What is wrong is that the usual derivation of $\mathbf{v_d}$ is non-relativistic. For planar geometry, the correct approach to the derivation of $\mathbf{v_d}$ involves use of a Lorentz transformation (Longmire, 1963, p. 30; Jackson, 1975, pp. 582-584), which can eliminate the component of $\mathbf{E}$ perpendicular to $\mathbf{B}$, yielding the usual $\mathbf{E} \times \mathbf{B}$ drift result, only if $E < Bc$. If $E > Bc$, a Lorentz transformation to a frame moving at velocity $\mathbf{E} \times \mathbf{B}/E^2$ (rather than $\mathbf{E} \times \mathbf{B}/B^2$) now eliminates the component of $\mathbf{B}$ perpendicular to $\mathbf{E}$. In this frame, particles now accelerate indefinitely parallel to $\mathbf{E}$, so no magnetic-insulation effect is predicted. The situations treated here do not involve probe potentials large enough to produce strong relativistic effects, but what is instead implied is that orbit curvatures due to the magnetic field become so slight that electron motions become dominated by electric-field inhomogeneities associated with the rotational symmetry of the probe's potential distribution. Therefore, the non-relativistic magnetic-bottle analysis of Section 2 still applies, and still predicts that radially-inward motion toward a probe will eventually be limited, except for particles having a zero value of the canonical angular momentum component J defined in Eq. (2). Palmadesso (paper appearing later in these Proceedings) has numerically calculated particle orbits in model spherical-probe sheath potentials in magnetic fields, and these orbits display both of the phenomena just described, namely the breakdown of $\mathbf{E} \times \mathbf{B}$ drift in strong electric fields, and the limitation of the resulting radially-inward motion because of conservation of J. The same phenomena are visible also in results from the NASCAP/LEO simulation of SPEAR I flight conditions, presented by Katz *et al* (1989). We have reproduced their Figures 8(a) and (b) herein as Figures 16(a) and (b). Figure 16(a) shows their calculated bipolar-sheath potential contours for a $46kV$ bias on one spherical probe and a $-6kV$ assumed floating potential for the SPEAR I rocket body. Figure 16(b) shows the trajectory of an electron in the potential of Figure 16(a). A sudden transition from $\mathbf{E} \times \mathbf{B}$ drift motion to accelerated motion is clearly visible, as also is orbital motion caused by nonzero angular momentum, closer to the probe.

7. PHENOMENA AROUND LARGE ORBITING OBJECTS AT HIGH VOLTAGES

Our discussion so far has been directed primarily toward rocket experiments involving large positive electrode voltages. In such experiments, effects of spacecraft motion (relative plasma drift) on sheath structure and current collection are generally thought to be unimportant. A very different situation arises in the planned Electrodynamic Tether experiment, which is part of the Shuttle-borne Tethered Satellite System (T.S.S.). In this experiment, it is planned to deploy an insulated conductive tether of up to $20km$ length, extended vertically upward from the Orbiter's cargo bay. At the end of the tether is to be located a conductive spherical subsatellite. One expected consequence of this arrangement is the generation of large-scale systems of low-frequency plasma waves in the ionosphere (Banks *et al*, 1981; Raitt *et al*, 1983; Grossi, 1984; Rasmussen *et al*, 1985; Urrutia and Stenzel, 1989; Stenzel and Urrutia, 1989). Another experimental objective, more closely related to our present discussion, is to investigate whether induced currents in the tether due to its motion across the geomagnetic field can provide a useful source of electric power in space.

This depends on achieving as large as possible an electron current collection by the subsatellite, either passively or with the aid of a low-energy plasma source known as a "plasma contactor". Here we consider only passive current collection; the performance of plasma contactors is analysed in four papers, by Hastings, Wilbur and Williams, Katz and Davis, and Cooke, respectively, which appear later in these Proceedings. In the Orbiter's reference frame, the ambient plasma contains an upwardly-directed $\mathbf{v} \times \mathbf{B}$ electric field of about $0.24 V/m$, where $\mathbf{v}$ is the Orbiter's orbital velocity. The Orbiter is to carry an electron emitter (Banks et al, 1981; Raitt et al, 1983) which is intended to keep its potential close to that of its surroundings. The subsatellite will then acquire a potential up to about $5kV$ positive with respect to its surroundings.

The planned diameter of the subsatellite is $1.4m$ (Raitt et al, 1983). Much larger subsatellites (conductive balloons) have also been considered (Williamson and Banks, 1976; Banks et al, 1981). In either event, the subsatellite's radius will be large compared with both the average gyroradius and the Debye length of ambient electrons. The situation around the subsatellite therefore appears likely to be similar to that analyzed by Sanmartin (1970; our Section 3), except that the ions and electrons will now have a drift speed $U = 8km/sec$ relative to the subsatellite. Since the mean thermal speeds $\bar{v}_i$ and $\bar{v}_e$ of ambient ions and electrons are roughly $1km/sec$ and $300km/sec$, respectively, drift effects would appear likely to be important for ions but negligible for electrons. However, in the case of electrons, this conclusion turns out to be untrue. The following discussion is based in large part on a treatment by Thompson (1985), and also on unpublished work by W.B. Thompson.

In the nondrifting situation analyzed by Sanmartin (1970; our Section 3), electron depletion by the probe created a positive potential disturbance which extended in both directions along the probe's magnetic shadow without attenuation until distances of the order of an electron mean free path were reached. However, in low-Earth-orbit conditions, electrons drift at speed U toward the upstream surface of this positive-potential region. They then enter this region, migrate along it to the subsatellite, and are collected. The flux associated with this drift, integrated over this surface out to a distance of order $L = D\bar{v}_e/U$ in both directions from the subsatellite, where $D = 2r_p$ is the subsatellite's diameter, then supplies the subsatellite's electron collection current. The speed and direction of this drift will be modified near this surface by electric fields associated with the potential change across it. The upstream surface of the positive-potential region (on each side of the subsatellite) now is no longer parallel to $\mathbf{B}$ but is "swept back" relative to $\mathbf{B}$ by a small angle $\theta \approx \tan^{-1}(U/\bar{v}_e)$ (Fig. 17). This implies that the region of positive potentials now tapers to zero width in a distance of order L along each of the directions parallel and antiparallel to $\mathbf{B}$. This distance will be large compared to D, but generally much smaller than the electron mean-free-path, so in this situation, a self-consistent collisionless treatment can be formulated. Positive ions striking the upstream side of this region reflect forward from it (Fig. 17), creating conditions conducive to two-stream instability just forward of it. Whether such instability has any substantial effect on electron collection has not been determined. The same repulsion of ions from the positive-potential region also creates an extensive ion-depleted wake region on its downstream side, and this wake region can be expected to contain negative potentials (Fig. 17). In Thompson's description, the total length of this wake region parallel to $\mathbf{B}$, $i.e.$ transverse to the relative plasma drift, will be of order $2L$.

From our viewpoint, the most important question regarding the treatments of Sanmartin (1970) and Thompson (1985) is whether they lead to different predictions for electron collection by the subsatellite. Sanmartin's theory includes collisions, and therefore leads to the populating of orbits which have negative total energies with respect to space potential and therefore cannot be populated by particles moving collisionlessly from infinity. In fact, the electron population reaching the probe in Sanmartin's treatment is a Maxwellian, with a reduced density factor [his Eq. (65)]

which at the probe depends on position perpendicular to **B** (our r coordinate in Section 2 and elsewhere). Therefore, in Sanmartin's description, most of the electron current reaching the probe is carried by negative-total-energy electrons.

The collisionless description given by Thompson (1985), and summarized above, is very different. In this description, the definition of space potential is more complicated because in a reference frame fixed on the subsatellite, there exists an ambient **v** × **B** electric field of about $0.24V/m$. However, this does not substantially affect what we can conclude about the velocity distribution of electrons reaching the subsatellite. This remains as follows: all electron orbits not connecting back to infinity are unpopulated. This includes all negative-total-energy orbits, and also those positive-total-energy orbits which are caused to return to the subsatellite by electric or magnetic fields. The positive-total-energy orbits which connect back to infinity have populations which are a function of their ambient velocities. This function is just the drifting Maxwellian velocity distribution of the ambient plasma. However, the drift velocity of these electrons is, as we have seen, very small compared to their mean thermal velocity, and even though this "small" amount of drift is crucial to the construction of a self-consistent collisionless treatment, it nonetheless has a negligible effect on the population of those orbits which connect back to infinity. This population can therefore be regarded as isotropic, *i.e.* dependent only on the total energy of each electron impacting the subsatellite, and this energy is conserved along the electron's orbit, again assuming that the electron has not passed through a region of significant time-dependent fluctuations (Section 4). If this is the case, we then have complete knowledge of the velocity distribution of impacting electrons if we know the "cutoff boundaries" in velocity space which separate the orbits which connect back to the ambient plasma from those which do not (Laframboise and Parker, 1973). This last question in turn is easy to resolve if electron acceleration into the positive-potential region is adiabatic (gyroradius $<<$ scale of changes in the electric field **E**), because the cutoff boundary is then "one-dimensional", *i.e.*, if the z direction is again parallel to **B**, electron orbits arriving at the subsatellite surface are populated only for v_z values such that $\frac{1}{2}m_e v_z^2 - e\phi_p > 0$, where ϕ_p is the subsatellite's potential relative to space (Laframboise and Parker, 1973; Laframboise and Rubinstein, 1976; Rubinstein and Laframboise, 1982; see also Section 2). All of this now implies that with these approximations, the velocity distribution of impacting electrons is just an "accelerated half-Maxwellian", and the electron current collected by the subsatellite is just the random current collected by the projection of its area onto a plane perpendicular to **B**. The dimensionless current i defined in Eq. (7) is then just equal to $\frac{1}{2}$.

However, this estimate may be much too small, because it excludes any correction for nonadiabatic effects on electron motions near the subsatellite; these were discussed in Section 2. It may seem surprising that such effects should be significant, because the average ambient-electron gyroradius $\bar{a}$ is much smaller than the subsatellite radius r_p. For $r_p = 0.7m$, $B = 0.3G = 3 \times 10^{-4}T$, and $kT_e = 0.1eV$, the ratio $\beta = r_p/\bar{a}$ defined following Eq. (10) is equal to 22.2. In spite of this, for a subsatellite potential $\phi_p = 5keV$, The Parker-Murphy (1967) upper-bound value for i, given by either Eq. (7) or the first two terms of Eq. (11), is 11.86; the correction given by the third term of Eq. (11) is insignificant. For this value of β and for the value $\psi_p = 5 \times 10^4$ implied by the parameter values just given, the numerical results of Sonmor given in Fig. 7 appear to indicate that the actual current will be very close to this upper-bound value. One cannot infer a firm conclusion on this point because the Sonmor results are for a Laplace potential distribution (infinite Debye length), rather than for the actual sheath potential distribution around the subsatellite, and no clear information exists on whether actual currents will be larger or smaller than the corresponding Laplace-limit currents (Sections 2 and 5). Nonetheless, the wide disparity between the values of $\frac{1}{2}$ and 11.86, given just above for i, suggests that nonadiabatic effects on electron motions near the subsatellite are very strong, and therefore the actual velocity-space cutoff boundary for electrons ar-

riving at the subsatellite is very different from that given by the "one-dimensional" cutoff-boundary relation noted above. However, this conclusion in turn could be affected strongly by the breakup of magnetic bottles into disjoint regions, which we noted in Section 5 and in Fig. 15, so it still requires detailed numerical verification.

For increasingly large subsatellite diameters D, the half-length L of the positive-potential region increases in proportion. It is instructive to ask at what value of D does L become large enough that a transition will occur from the collisionless description of Thompson (1985) to the collisional one of Sanmartin (1970). To calculate the electron mean-free-path, we use the classical Spitzer (1962, Chapter 5) results for the electron collision frequency in a fully-ionized gas. To use these results, we consider an electron "test particle" whose velocity v_e is given by $mv_e^2 = 3kT_e$, i.e. which has kinetic energy equal to the average value for electrons at temperature T_e.

We include contributions to its cumulative angular scattering from both ambient electrons and ambient ions. For ambient-electron density $n_e = 10^5/cm^3$ and temperature $T_e = 0.1eV$, Eq. (5.22) of Spitzer (1956) gives an electron mean-free-path $\lambda_e = 725m$ for cumulative angular scattering. We have just seen that the most important distinction between the collisionless and collisional descriptions is likely to be the energy distribution of electrons in the positive-potential regions. Another important mean-free-path therefore is that for energy exchange among electrons, also defined by Spitzer (1956, Eq. 5.25). Bearing in mind that electron-electron encounters change the electron energy distribution much more rapidly than do electron-ion encounters, a recalculation of Table 5.3 of Spitzer (1956) to include ion effects indicates that the energy-exchange mean-free-path is only moderately larger than λ_e for most electrons.

A good approximate criterion for collisionless current collection by the subsatellite therefore is that $L << \lambda_e$. With the above-mentioned relation $L = D\overline{v}_e/U$ and the values $U = 8km/sec$ and $\overline{v}_e = 300km/sec$, this criterion reduces to $D << 19m$. This result implies that collisional effects can become significant for balloon subsatellite diameters which are within the realm of possibility.

In rocket experiments, U is generally much smaller, and this criterion then becomes much more severe. For $U = 1km/sec$, we obtain $D << 2.4m$. The SPEAR I probes (Sections 3, 4, and 6), whose diameters were $20cm$, are comfortably within this limit, so we infer that even the relatively small amount of spacecraft motion present in the SPEAR I experiment was enough to ensure that current collection by these probes was essentially a collisionless process. The collecting portion of the CHARGE-2 daughter payload (Myers et al, 1989) was somewhat larger, with a largest dimension of 82 cm, but was still within the above-mentioned approximate limit. As mentioned in Sections 3 and 4, current collection in both experiments appeared to be described well by collisionless, steady-state theory. A surprising prediction of the discussion in this Section is the extreme sensitivity of this conclusion to very small values of ambient-electron drift motion. The effects of this drift motion appear to remove the apparent contradiction between the conclusion of most of our discussion in Section 3 (which applied in the strict absence of drift) and the apparent success of collisionless, steady-state theory in both of these experiments. To put this interpretation on a firmer basis will require the development of a theory which is capable of making quantitative predictions of collected current in the transitional regime between the collisionless situation described by Thompson (1985) and the collisionally-influenced one of Sanmartin (1970).

8. CONCLUSIONS

Our discussion in Sections 2-7 has revealed subtle and surprising aspects of the problem of predicting current collection by probes in the space magnetoplasma. Many of these aspects involve unresolved issues. They include the following:

(1) The attraction-region current-voltage characteristic of a probe in a magnetoplasma can contain a "negative-resistance region" near space potential (Section 2).

(2) Numerical calculations of collisionless, steady-state, Laplace-limit currents indicate that these remain substantially below the canonical-upper-bound current values even at large attractive potentials. Implications for current collection in more realistic potentials are not clear (Sections 2 and 5).

(3) In a nondrifting plasma, no current-collection theory is possible which includes space-charge effects but not interparticle collisions, no matter how large the ambient charged-particle mean-free-paths are (Section 3). However, even a very small amount of relative plasma drift, such as that involved in a typical rocket experiment, can change this conclusion fundamentally (Section 7).

(4) Plasma turbulence appears to have an important influence on current collection by probes in fusion plasmas but not in space plasmas. Such turbulence is not understood well enough to explain why (Section 4).

(5) Space-charge effects, which tend to steepen the sheath potential profile near a probe, decrease attracted-particle collection in nonmagnetic situations, but may possibly increase it in magnetic ones (Section 2). However, formation of "bulges" and breakup of magnetic bottles into disjoint "bubble" regions by such space-charge effects may reverse this effect. Presently available experimental results and theory do not provide sufficient evidence to indicate whether an increase or a decrease actually occurs (Section 5).

(6) The existence of trapped-orbit regions around a probe provides pathways for additional current collection due to collisional ionization, collisional scattering, and possibly turbulent scattering. The first of these is undoubtedly important; no predictions are available for the other two (Section 5).

(7) Circumferential "$\mathbf{E} \times \mathbf{B}$ drifting" motion can break down in the strong electric fields that exist near a probe, and be replaced by radially-accelerated motion. This motion in turn can be limited by angular-momentum effects closer to the probe (Section 6).

ACKNOWLEDGMENTS

REFERENCES

Balmain, K.G., Probe-Triggered Audiofrequency Plasma Oscillations, IEEE Transactions on Antennas and Propagation AP-20, 400, 1972.

Banks, P.M., P.R. Williamson, and K.-I. Oyama, Electrical behavior of a Shuttle Electrodynamic Tether System (SETS), Planet. Space Sci. 29, 139, 1981.

Bernstein, I.B., and I.N. Rabinowitz, Theory of electrostatic probes in a low-density plasma, Phys. Fluids 2, 112, 1959.

Bienkowski, G.K., and K.-W. Chang, Asymptotic theory of a spherical electrostatic probe in a stationary weakly ionized plasma, Phys. Fluids 11, 784, 1968.

Bohm, D., E.H.S. Burhop, and H.S.W. Massey, The use of probes for plasma exploration in strong magnetic fields. In: The Characteristics of Electrical Discharges in Magnetic Fields, edited by A. Guthrie and R.K. Wakerling, pp. 13-76, McGraw-Hill, New York, 1949.

Chou, Y.S., L. Talbot, and D.R. Willis, Kinetic theory of a spherical electrostatic probe in a stationary plasma, Phys. Fluids 9, 2150, 1966.

Chung, P.M., L. Talbot, and K.J. Touryan, Electric Probes in Stationary and Flowing Plasmas: Theory and Application. Springer-Verlag, New York, 1975.

Cooke, D.L., and I. Katz, Ionization-induced instability in an electron-collecting sheath, J. Spacecraft and Rockets 25, 132, 1988.

Friedland, L., and Yu. M. Kagan, The theory of electron current to a spherical probe at intermediate pressures, J. Phys. D: Appl. Phys. 12, 739, 1979.

Godard, R., and J.G. Laframboise, Total current to cylindrical collectors in collisionless plasma flow, Planet. Space Sci. 31, 275, 1983.

Grossi, M.D., Spaceborne long vertical wire as a self-powered ULF/ELF radiator, IEEE Journal of Oceanic Engineering OE-9, 211, 1984.

Jackson, J.D., Classical Electrodynamics, 2nd Ed., Wiley, New York, 1975.

Katz, I., G.A. Jongeward, V.A. Davis, M.J. Mandell, R.A. Kuharski, J.R. Lilley, Jr., W.J. Raitt, D.L. Cooke, R.B. Torbert, G. Larson, and D. Rau, Structure of the bipolar plasma sheath generated by SPEAR I, J. Geophys. Res. 94, 1450, 1989.

Laframboise, J.G., Theory of spherical and cylindrical Langmuir probes in a collisionless, Maxwellian plasma at rest. Institute for Aerospace Studies, University of Toronto, Report No. 100, 1966.

Laframboise, J.G., and L.W. Parker, Probe design for orbit-limited current collection, Phys. Fluids 16, 629, 1973.

Laframboise, J.G., and Rubinstein, J., Theory of a cylindrical probe in a collisionless magneto-plasma, Phys. Fluids 19, 1900, 1976.

Lai, S.T., H.A. Cohen, K.H. Bhavnani, and M. Tautz, Sheath ionization model of beam emissions from large spacecraft. In: Spacecraft Environmental Interactions Technology 1983, edited by C.K. Purvis and C.P. Pike, NASA Conf. Publ. 2359/Rep. AFGL-TR-85-0018, pp. 253-262, Air Force Geophys. Lab., Hanscom Air Force Base, Mass., 1985.

Langmuir, I., and K.B. Blodgett, Currents limited by space charge between concentric spheres, Phys. Rev. 23, 49, 1924.

Linson, L.M., Current-voltage characteristics of an electron-emitting satellite in the ionosphere, J. Geophys. Res. 74, 2368, 1969.

Linson, L.M., Charge neutralization as studied experimentally and theoretically. In: Artificial particle beams in space plasma studies, edited by B. Grandal, pp. 573-595, NATO Advanced Study Institutes Series B: Physics, Volume 79, Plenum, New York, 1982.

Longmire, C.L., Elementary Plasma Physics, Wiley/Interscience, New York, 1963.

Maehlum, B.N., Beam-Plasma Experiments, Computer Physics Communications 49, 119, 1988.

Makita, H., and K. Kuriki, Comparative study of spherical and cylindrical drift probes. In: Proc. 10th International Symposium on Rarefied Gas Dynamics, edited by J. Leith Potter, pp. 1007-1014, Progress in Astronautics and Aeronautics, Vol. 51, Amer. Inst. of Astronautics and Aeronautics, New York, 1977.

Makita, H., and K. Kuriki, Current collection by spherical Langmuir probes drifting in a collisionless plasma, Phys. Fluids 21, 1279, 1978.

Mott-Smith, H.M., and I. Langmuir, The theory of collectors in gaseous discharges. Phys. Rev. 28, 727, 1926.

Murphy, G.B., J. Pickett, N. D'Angelo, and W.S. Kurth, Measurements of plasma parameters in the vicinity of the space shuttle, Planet. Space Sci. 34, 993, 1986.

Myers, N.B., W.J. Raitt, B.E. Gilchrist, P.M. Banks, T. Neubert, P.R. Williamson, and S. Sasaki, A comparison of current-voltage relationships of collectors in the Earth's ionosphere with and without electron beam emission, Geophys. Res. Lett. 16, 365, 1989.

Papadopoulos, K., and E.P. Szuszczewicz, Current understanding and issues on electron beam injection in space, COSPAR General Assembly 1986.

Parker, L.W., and B.L. Murphy, Potential buildup on an electron-emitting ionospheric satellite, J. Geophys. Res. 72, 1631, 1967.

Parker, L.W., Computer Solutions in Electrostatic Probe Theory. I. Spherical Symmetry with Collisions. Air Force Avionics Laboratory, Wright-Patterson Air Force Base, Ohio, Report No. AFAL-TR-72- 222, Part 1, 1973.

Parker, L.W., Computer Method for Satellite Plasma Sheath in Steady-State Spherical Symmetry, Air Force Geophysics Laboratory, Hanscom Air Force Base, Mass., Report No. AFCRL-TR-75-0410, 1975.

Raitt, W.J., P.M. Banks, and P.R. Williamson, Electrodynamic tether experiments in the ionosphere. In: Active Experiments in space, edited by W.R. Burke, European Space Agency Publ. ESA SP-195, pp. 361-367, 1983.

Rasmussen, C.E., P.M. Banks, and K.J. Harker, The excitation of plasma waves by a current source moving in a magnetized plasma: the MHD approximation, J. Geophys. Res. 90, 505, 1985.

Rubinstein, J., and J.G. Laframboise, Upper-bound current to a cylindrical probe in a collisionless magnetoplasma, Phys. Fluids 21, 1655, 1978.

Rubinstein, J., and J.G. Laframboise, Theory of a spherical probe in a collisionless magnetoplasma, Phys. Fluids 25, 1174, 1982.

Rubinstein, J., and J.G. Laframboise, Theory of axially symmetric probes in a collisionless magnetoplasma: aligned spheroids, finite cylinders, and disks, Phys. Fluids 26, 3624, 1983.

Sanmartin, J.R., Theory of a probe in a strong magnetic field, Phys. Fluids 13, 103, 1970.

Self, S.A., and C.H. Shih, Theory and measurements for ion collection by a spherical probe in a collisional plasma, Phys. Fluids 11, 1532, 1968.

Shih, C.H., and E. Levi, Determination of the collision parameters by means of Langmuir probes, AIAA J. 9, 2417, 1971.

Spitzer, L., Jr., Physics of Fully Ionized Gases, Interscience, New York, 1956.

Stangeby, P.C., The interpretation of plasma probes for fusion experiments. In: Plasma Diagnostics, Vol. 2: Surface Analysis and Interactions, edited by O. Auciello and D.L. Flamm, pp. 157-209, Academic Press, San Diego, 1989.

Stangeby, P.C., and G.M. McCracken, Plasma boundary pheonomena in tokamaks, 1990 (submitted to Nucl. Fusion).

Stenzel, R.L., Instability of the sheath-plasma resonance, Phys. Rev. Lett. 60, 704, 1988.

Stenzel, R.L., and J.M. Urrutia, Whistler wings from moving electrodes in a magnetized laboratory plasma, Geophys. Res. Lett. 16, 361, 1989.

Szuszczewicz, E.P., and P.Z. Takacs, Magnetosheath effects on cylindrical Langmuir probes, Phys. Fluids 22, 2424, 1979.

Szuszczewicz, E.P., Controlled electron beam experiments in space and supporting laboratory experiments: a review, J. Atmos. Terrestrial Phys. 47, 1189, 1985.

Talbot, L., and Y.S. Chou, Langmuir probe response in the transition regime. In: Proc. 6th Internat. Symposium on Rarefied Gas Dynamics, edited by L. Trilling and H.Y. Wachman, pp. 1723-1737, Academic Press, New York, 1969.

Tanenbaum, B.S., Plasma Physics, McGraw-Hill, New York, 1967.

Thompson, W.B., Preliminary investigation of the electrodynamics of a conducting tether. In: Spacecraft Environmental Interactions Technology 1983, edited by C.K. Purvis and C.P. Pike, NASA Conf. Publ. 2359/Rep. AFGL-TR-85-0018, pp. 649-662, Air Force Geophys. Lab., Hanscom Air Force Base, Mass., 1985.

Thornton, J.A., Comparison of theory and experiment for ion collection by spherical and cylindrical probes in a collisional plasma, AIAA J. 9, 342, 1971.

Urrutia, J.M., and R.L. Stenzel, Anomalous currents to an electrode in a magnetoplasma, Phys. Rev. Lett. 57, 715, 1986.

Urrutia, J.M., and R.L. Stenzel, Transport of current by whistler waves, Phys. Rev. Lett. 62, 272, 1989.

Wasserstrom, E., C.H. Su, and R.F. Probstein, Kinetic theory approach to electrostatic probes, Phys. Fluids 8, 56, 1965.

Whipple, E.C., Jr., The equilibrium electric potential of a body in the upper atmosphere and in interplanetary space, Ph.D. Thesis, George Washington University/NASA Goddard Space Flight Center, Greenbelt, Maryland, Report No. X-615-65-296, 1965.

Williamson, P.R., and P.M. Banks, The tethered balloon current generator: A space shuttle tethered subsatellite for plasma studies and power generation, Final Report, NOAA, 1976.

Winckler, J.R., The application of artificial electron beams to magnetospheric research, Rev. Geophys. Space Phys. 18, 659, 1980.
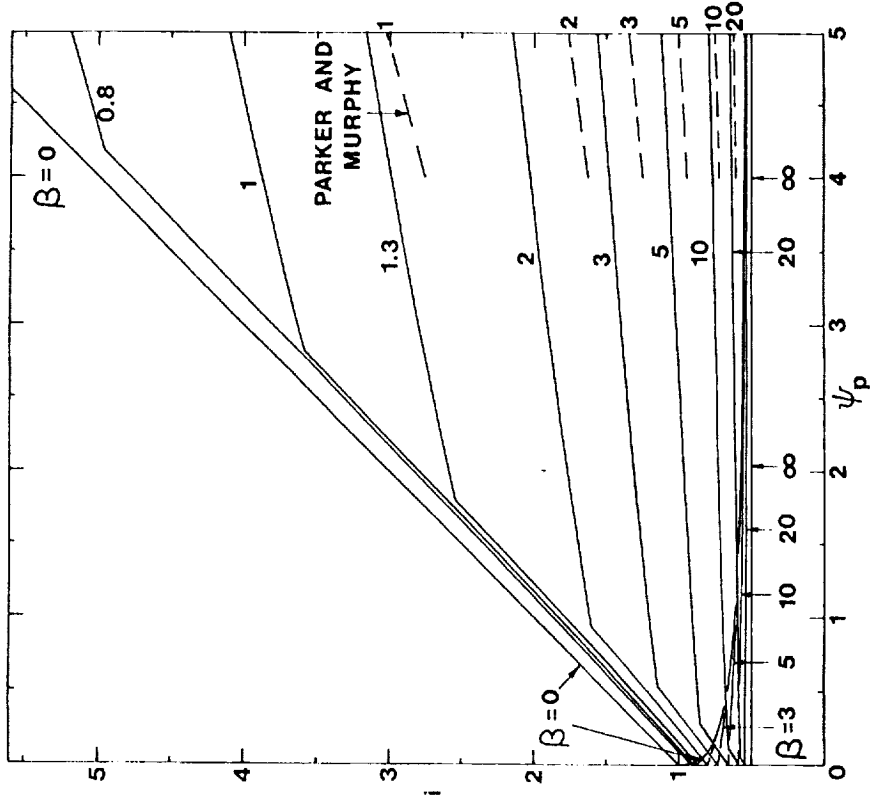
Figure 2. Dimensionless attracted-particle current $i = I/[4\pi r_p^2 q n_\infty (kT/2\pi m)^{1/2}]$, versus dimensionless probe potential $\psi_p = -q\phi_p/kT$, for various values of dimensionless magnetic-field strength $\beta = r_p/\overline{r_L}$. The increasing and decreasing curves represent least-upper-bound and adiabatic-limit currents, respectively. In the limit $\beta \to \infty$, these currents coincide; otherwise, the question of which curve is closer to the actual current is discussed in Section 2. Note the rapidly increasing disparity between these two sets of curves as ψ_p increases. The increasing curve for $\beta = 0$ is the Mott-Smith and Langmuir (1926) orbit-limited-current result. The portions of the increasing curves to the left and right of the "kinks" (discontinuities of slope) in these curves represent "helical" and canonical upper-bound currents (Section 2), respectively. Reproduced from Figure 8 of Rubinstein and Laframboise (1982).
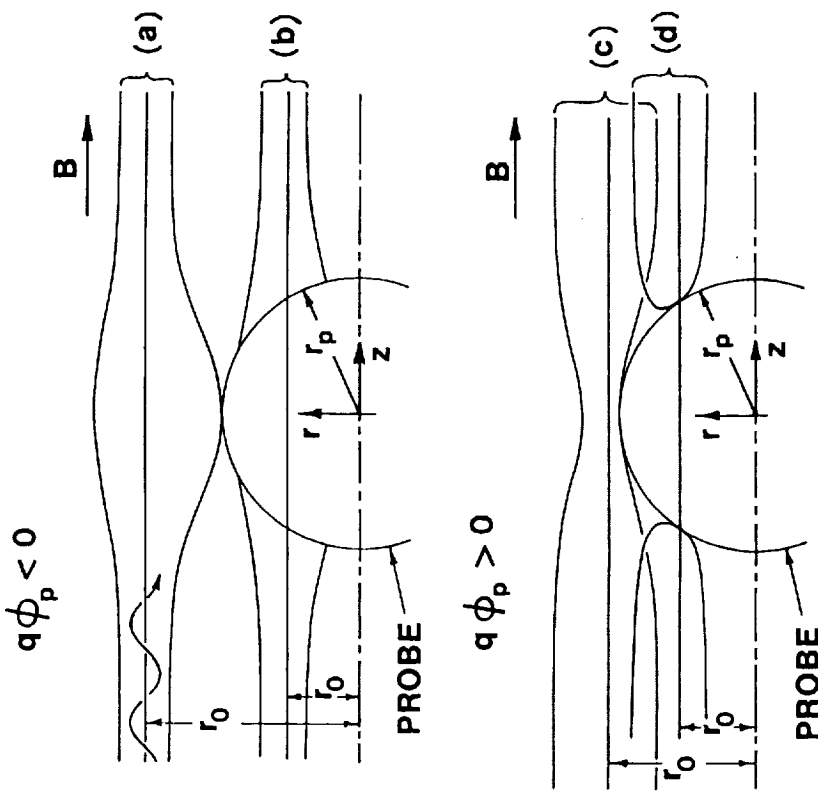
Figure 1. General appearance of "magnetic bottles" for attractive [(a), (b)] and repulsive [(c), (d)] probe potentials, for $r_o > r_p$ [(a), (c)] and $r_o < r_p$ [(b), (d)], where r_p is the probe radius and r_o is defined in Eq. (5). In (a), (c), and (d), the bottles shown just touch the probe. All bottles have rotational symmetry about the z axis. The bottle shapes are the same for particle orbits encircling or nonencircling the z axis (Section 2; Rubinstein and Laframboise, 1982, Section IV). Also shown is a typical nonencircling orbit far from the probe; note that if the orbit has nonzero pitch, it does not touch the bottle boundary in general. Reproduced from Figure 6 of Rubinstein and Laframboise (1982).

37
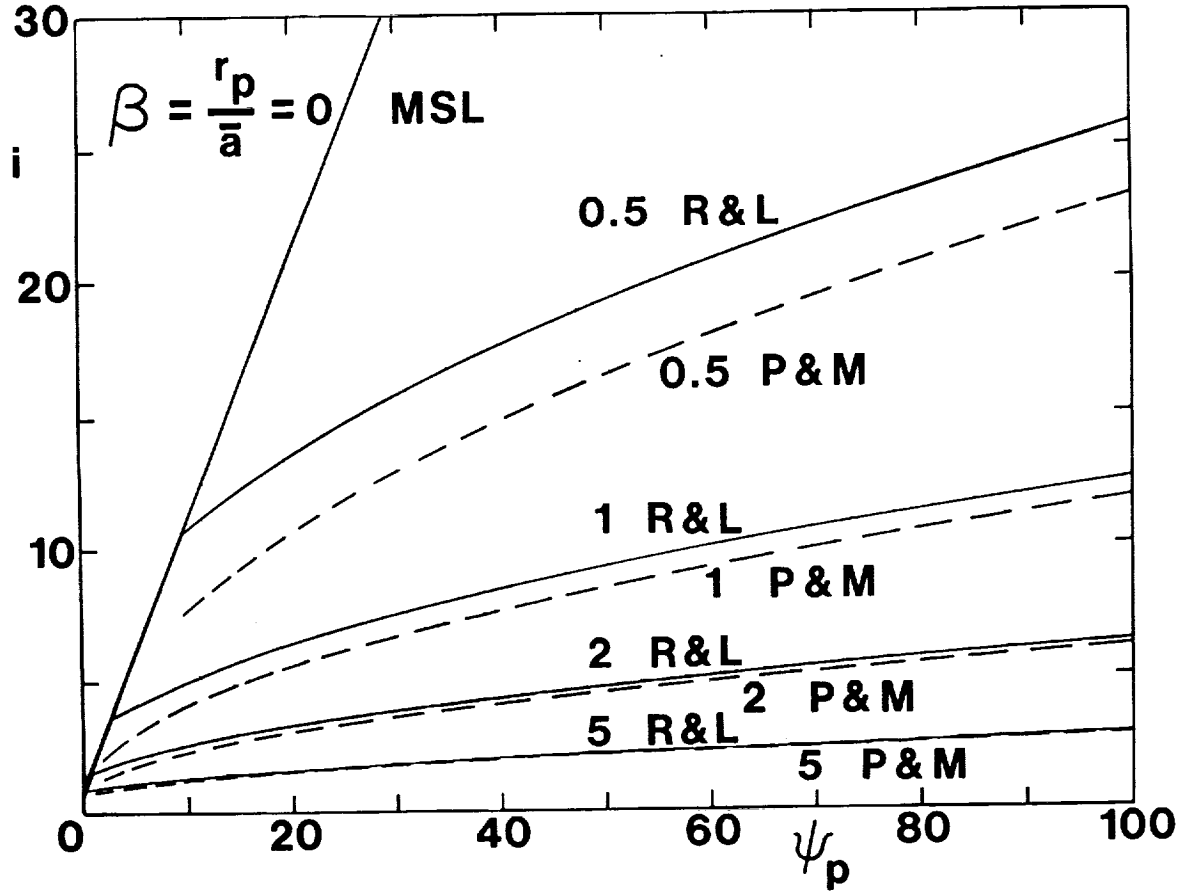
Figure 3. Comparison of the Rubinstein-Laframboise [1982; solid curves; given by our Eqs. (8) - (10)] and Parker-Murphy [1967; dashed curves; given by our Eq. (7)] canonical-upper-bound values for dimensionless attracted-particle current i as a function of dimensionless probe potential ψ_p, for various values of the dimensionless magnetic-field strength β. The curve for $\beta = 0$ is the Mott-Smith and Langmuir (1926) orbit-limited-current result.
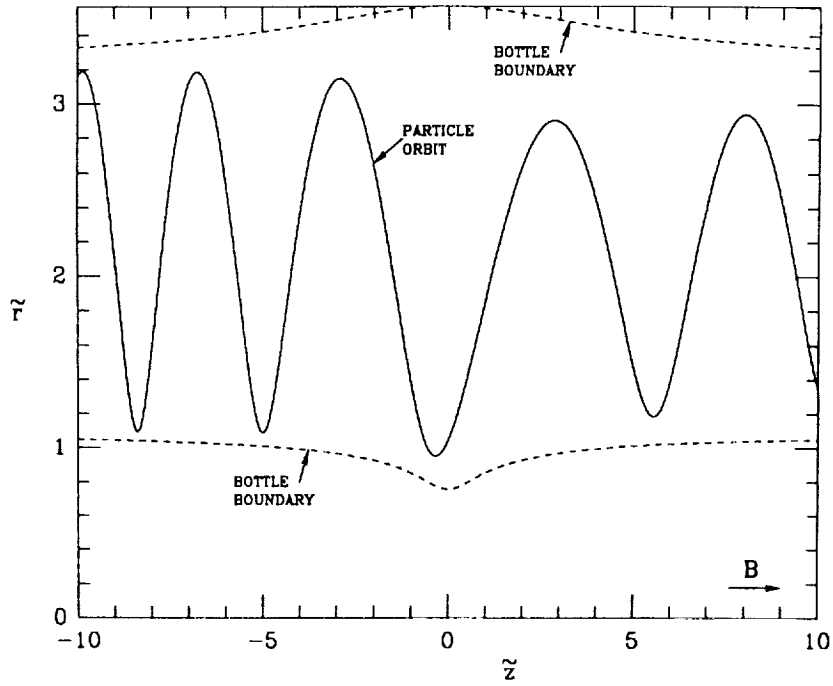
Figure 4(a). Results of L.J. Sonmor (Ph.D. thesis, in preparation), for the trajectory in scaled coordinates $[\tilde{r} = r(|m\phi_p\, r_p/qB^2|)^{1/3}, \tilde{z} = z(|m\phi_p r_p/qB^2|)^{1/3}]$ of a charged particle in an attractive Coulomb electric field and uniform magnetic field, given by numerical solution of Eq. (14). Also shown are the boundaries of allowed motion ("magnetic bottle boundaries") for the same particle, implied by conservation of energy and canonical angular momentum. The $\tilde{z}$ axis (parallel to the magnetic field) has been compressed for purposes of display. The portions of the trajectory which are outside the plot boundary are monotonic progressions in $\tilde{z}$ from and to infinity. The initial conditions are: $\tilde{z} = -20$, $d\tilde{z}/d\tau = \sqrt{0.17}$, scaled radius $\tilde{r}_0$ of guiding centre $= \sqrt{4.6}$, scaled gyroradius $= \sqrt{2.2}$, and phase angle $= 0$.
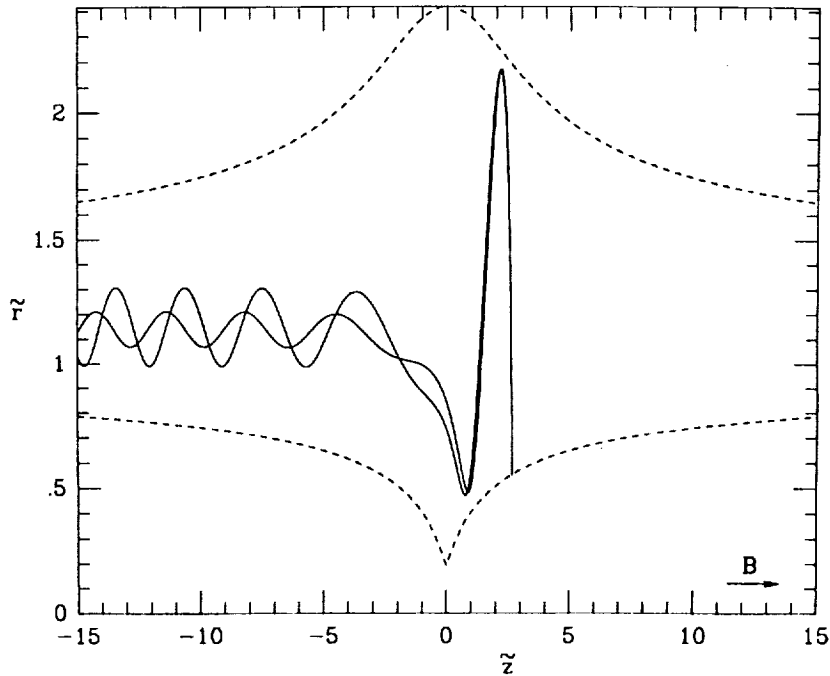
Figure 4(b). Same as Fig. 4(a), except that the initial conditions are: $\tilde{z} = -20$, $d\tilde{z}/d\tau = \sqrt{0.15}, \tilde{r}_0 = \sqrt{1.3}$, scaled gyroradius $= \sqrt{0.02}$, and phase angle $= 0$.
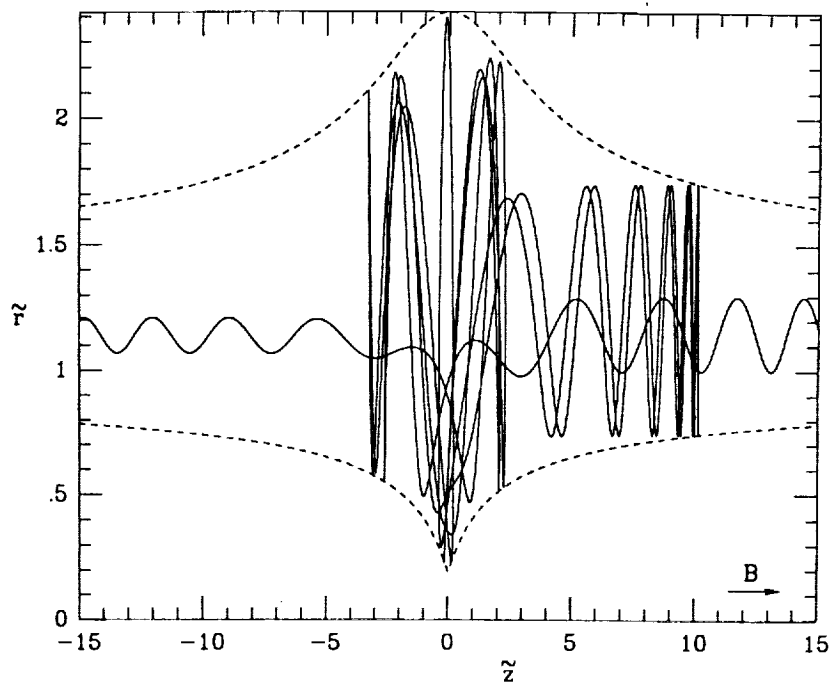
Figure 4(c). Same as Fig. 4(b), except that the initial phase angle is $7\pi/32$.
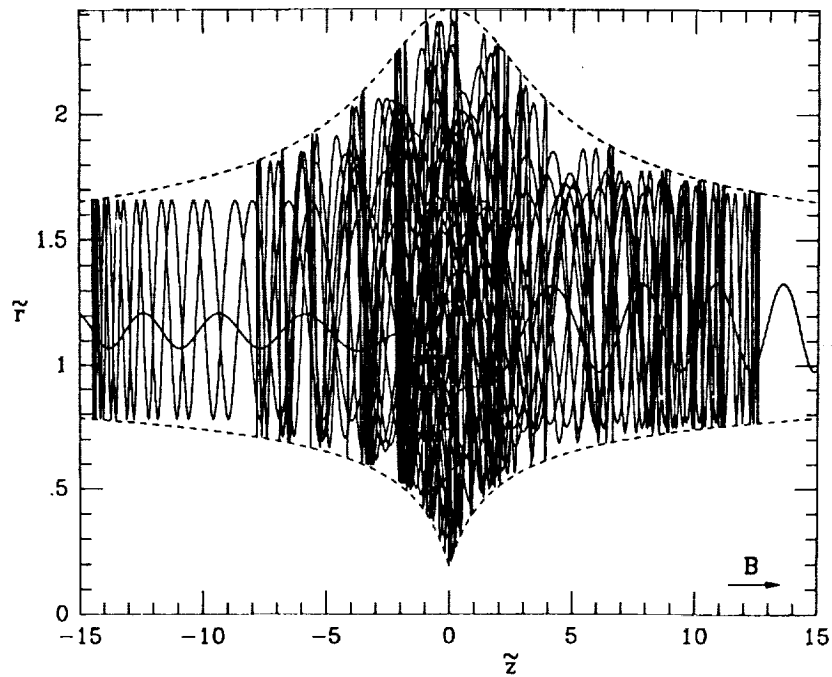
Figure 4(d). Same as Fig. 4(b), except that the initial phase angle is $11\pi/32$.
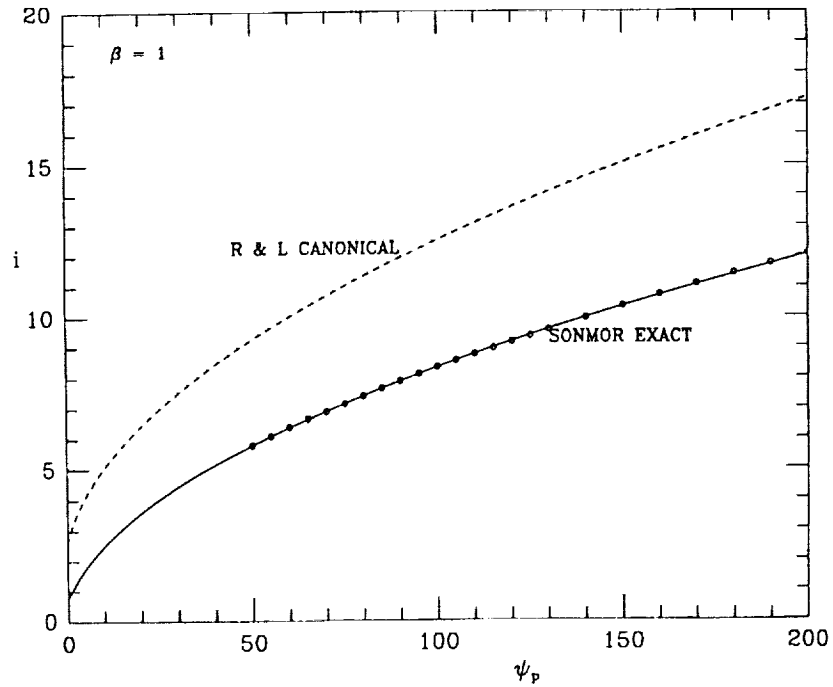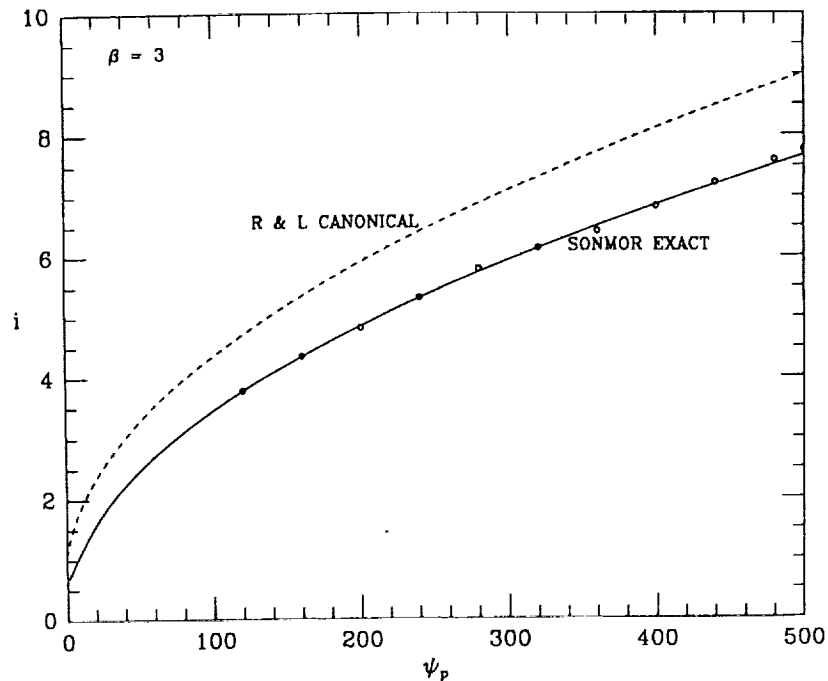
40
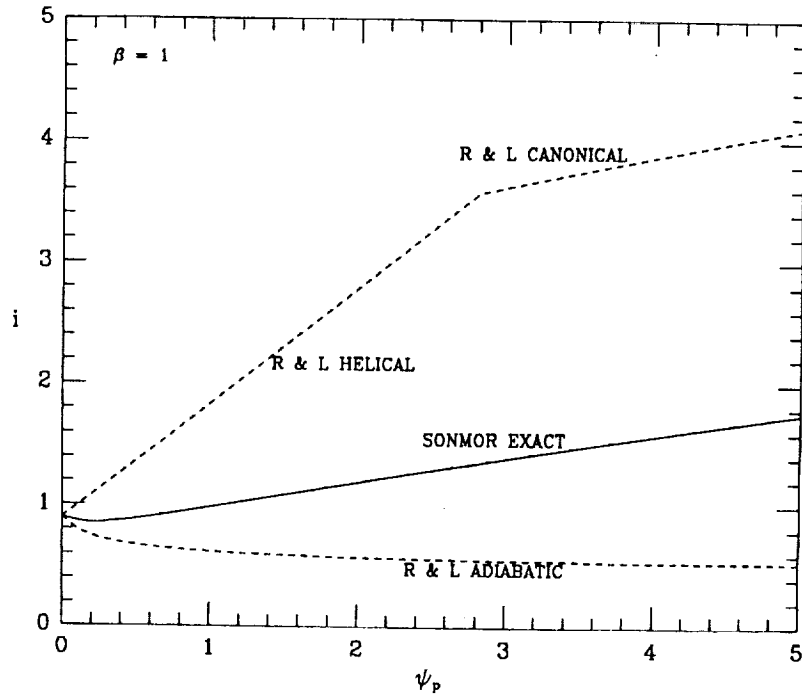
Figure 5(a). Dimensionless attracted-particle current i versus dimensionless probe potential ψ_p for a ratio β of probe radius to average ambient attracted-particle gyroradius of 1. Also displayed are the adiabatic-limit currents and the smaller of the helical upper-bound and canonical upper-bound currents, calculated by Rubinstein and Laframboise (1982).
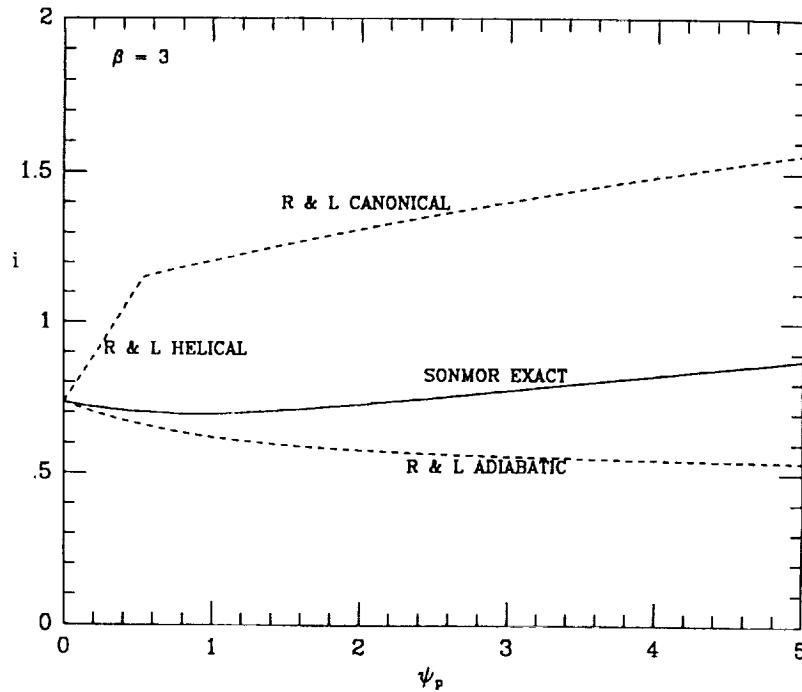
Figure 5(b). Same as Fig. 5(a), except that $\beta = 3$.

41

Figure 6(a). Dimensionless attracted-particle current i versus dimensionless probe potential ψ_p for a ratio β of probe radius to average ambient attracted-particle gyroradius of 1, plotted for a larger range of probe potentials than in Fig. 5(a). Also displayed is the canonical upper-bound current due to Rubinstein and Laframboise (1982). The minimum in the exact current at $\psi_p \approx 0.2$, which was evident in Fig. 5(a), is only barely visible here. Here and in Fig. 6(b), numerical errors in the "exact" results at larger ψ_p are noticeable on the scale of these graphs, and we have therefore marked actual computed values for larger ψ_p by open circles, and a curve-fit to them by a solid line.

Figure 6(b). Dimensionless attracted-particle current i versus dimensionless probe potential ψ_p for a ratio β of probe radius to average ambient attracted-particle gyroradius of 3, plotted for a larger range of probe potentials than in Fig. 5(b). Also displayed is the canonical upper-bound current due to Rubinstein and Laframboise (1982). The minimum in the exact current at $\psi_p \approx 0.9$, which was evident in Fig. 5(b), is only barely visible here.
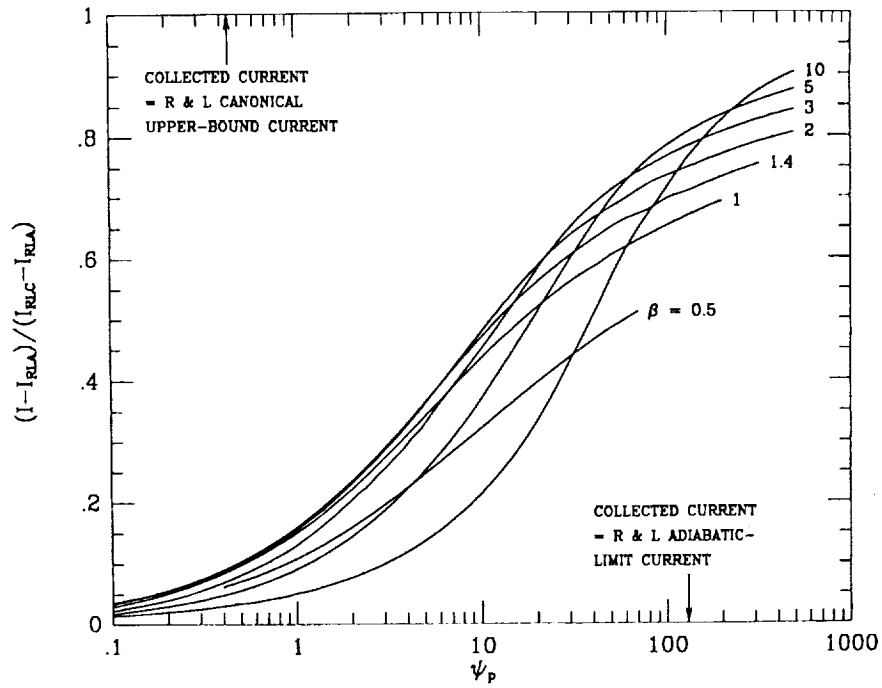
Figure 7. Computed results of L.J. Sonmor (Ph.D. thesis, in preparation), showing transition from adiabatic-limit current toward canonical upper-bound current as probe potential ψ_p becomes more attractive, for various ratios β of probe radius to average ambient attracted-particle gyroradius. I_{RLA} and I_{RLC} are the adiabatic-limit current and the canonical upper-bound current, respectively, both due to Rubinstein and Laframboise (1982). The canonical upper-bound current is also given by Eqs. (8)–(10). In this Figure, the curves have been smoothed to reduce oscillations caused by numerical errors in individual results.
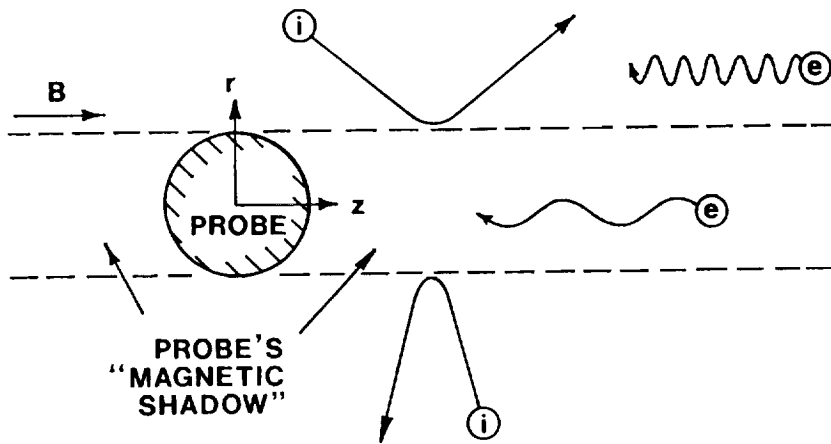
Figure 8. General appearance of representative collisionless ion and electron orbits far from the probe but not beyond the positive-potential disturbance (Sanmartin, 1970) which extends along the probe's magnetic shadow. Diagram is schematic only since this disturbance can extend very far in the z and $-z$ directions.

43
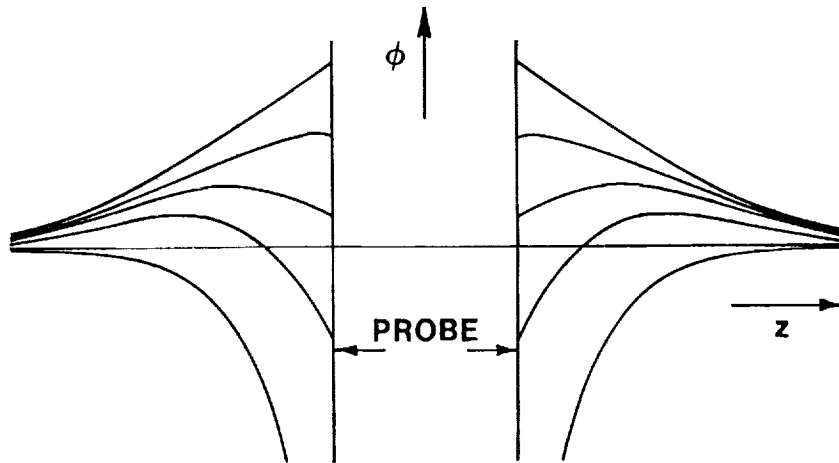
Figure 9. General appearance of potentials as a function of z for $r = 0$ under conditions analyzed by Sanmartin (1970) and described in Section 3.
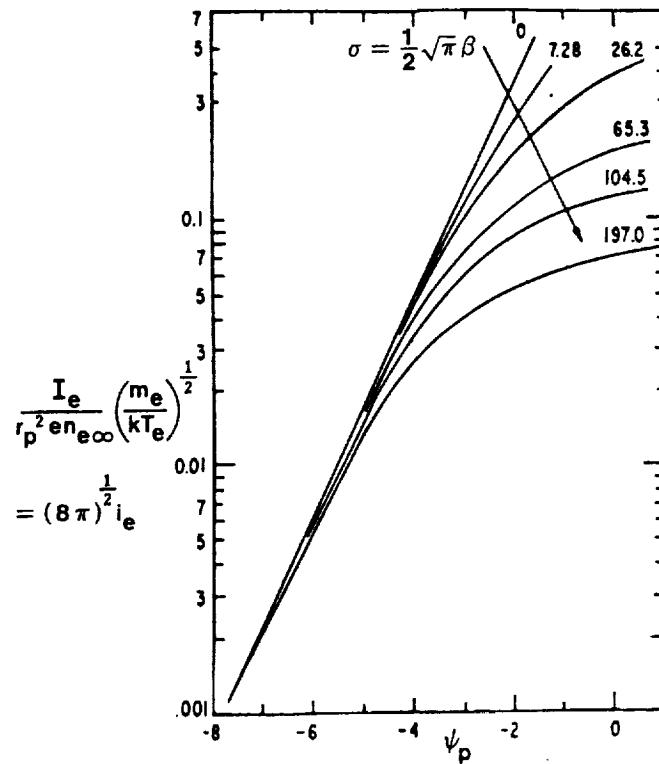

Figure 10. Reproduced from Fig. 1 of Sanmartin (1970), with notation changed, showing his results for electron current collection by a spherical probe in a magnetoplasma for which $T_i = T_e$ and containing singly-charged ions. Other assumptions made in Sanmartin's treatment are described in Section 3.
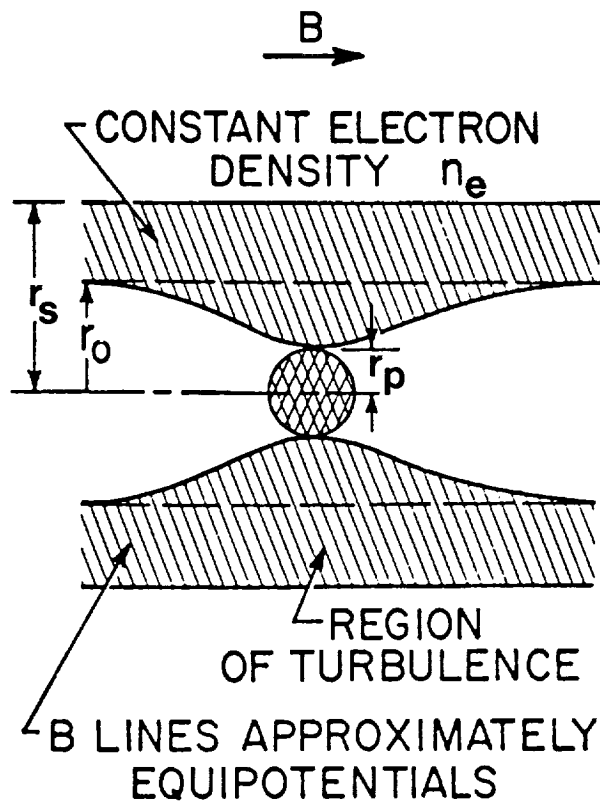
44

B
→

CONSTANT ELECTRON
DENSITY n_e

r_s

r_o

r_p

REGION
OF TURBULENCE

B LINES APPROXIMATELY
EQUIPOTENTIALS

Figure 11. Reproduced from Fig. 2 of Linson (1969), showing the construction of his constant-density cylindrical space-charge shielding model. r_o is the critical radius defined by his Eq. 8 (our Eq. 6).
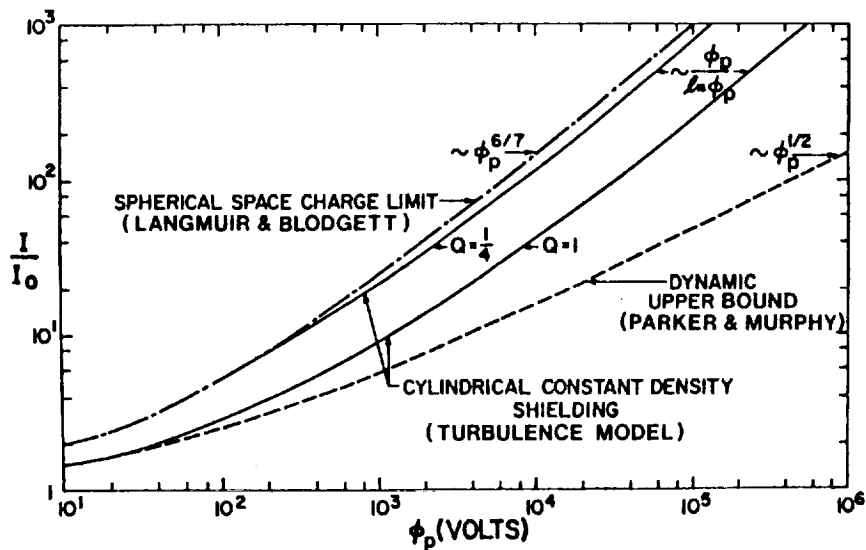
10^3

10^2

$\frac{I}{I_o}$

10^1

1

$\sim \frac{\phi_p}{\ln \phi_p}$

$\sim \phi_p^{6/7}$

$\sim \phi_p^{1/2}$

SPHERICAL SPACE CHARGE LIMIT
(LANGMUIR & BLODGETT)

$Q = \frac{1}{4}$ $Q = 1$

DYNAMIC
UPPER BOUND
(PARKER & MURPHY)

CYLINDRICAL CONSTANT DENSITY
SHIELDING
(TURBULENCE MODEL)

10^1 10^2 10^3 10^4 10^5 10^6

ϕ_p(VOLTS)

Figure 12. Reproduced from Fig. 3 of Linson (1970), with some notation changed, showing a comparison of current-versus-probe-voltage predictions from three models discussed by him. Their asymptotic behaviour for large probe voltage ϕ_p is shown. In this Figure, I_o equals one-half the random current I_R defined in our Section 2. The dot-dash curve represents the Langmuir-Blodgett (1924) spherical space-charge-limited current value. For constant potential, this current scales approximately as $I_o^{-4/7}$. The normalized voltage ϕ^* defined following our Eq. (19) is the same as the quantity ϕ_o defined in Linson's Eq. (8), and has been taken to be 178 volts, which is equivalent to $Br_p = 0.45Gm$. A change in the constant Q displaces the solid curve horizontally by the appropriate factor.
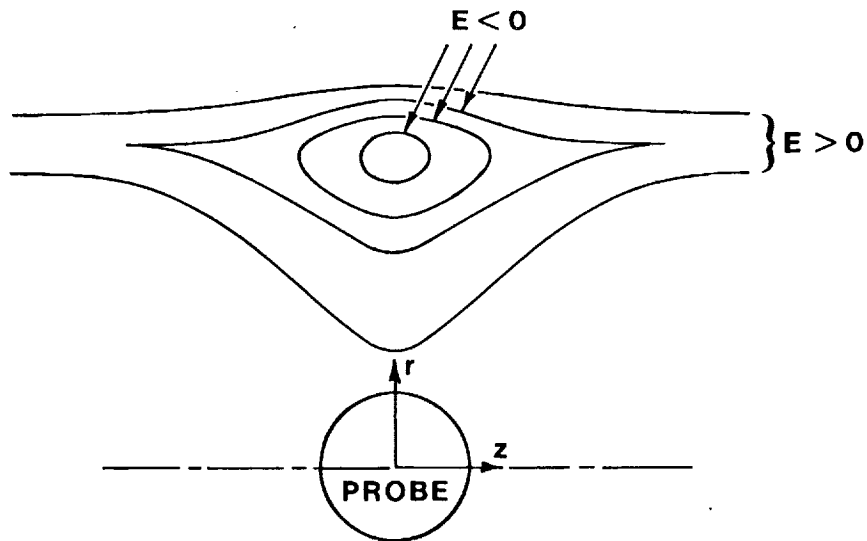
45

Figure 13. General appearance of open magnetic bottles corresponding to $E > 0$ and closed ones corresponding to $E < 0$, all for the same value of the canonical angular momentum component J about the z axis, defined in Eq. (2). Note the "pointedness" of bottles corresponding to slightly negative values of E.
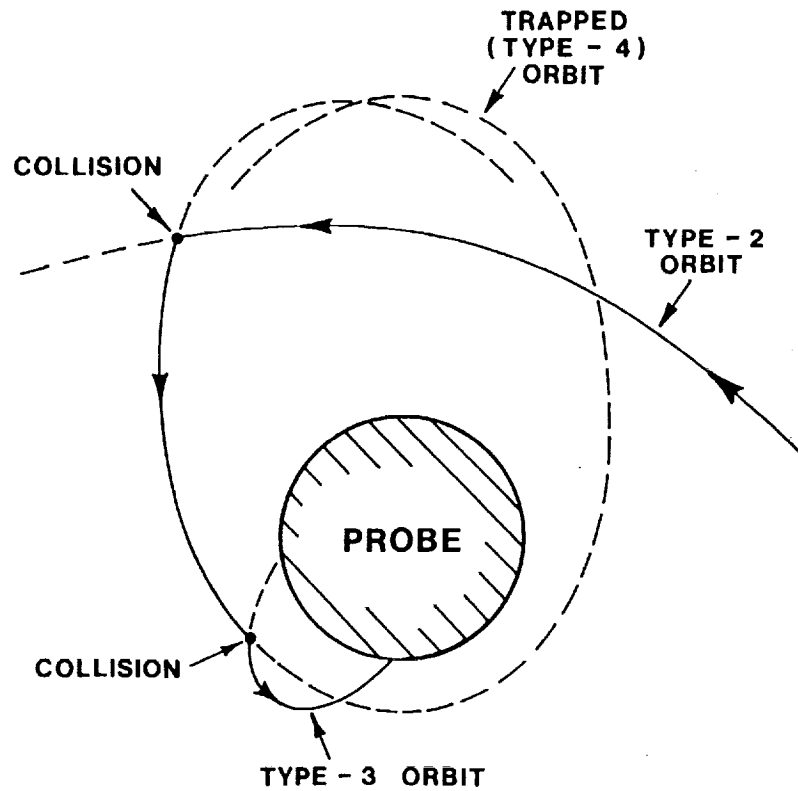

Figure 14. Illustration of how trapped orbits provide an additional current pathway to a probe. Whether trapped orbits exist depends on electric and magnetic fields present; if B is negligible, E must vary with r less steeply than r^{-3} for trapped orbits to exist (Section 5). The orbit classification shown is that due to Parker (1973, 1975); see preceding paper by E.C. Whipple in these Proceedings. In a magnetic field, the shapes of these orbits can be much more complicated than those shown.
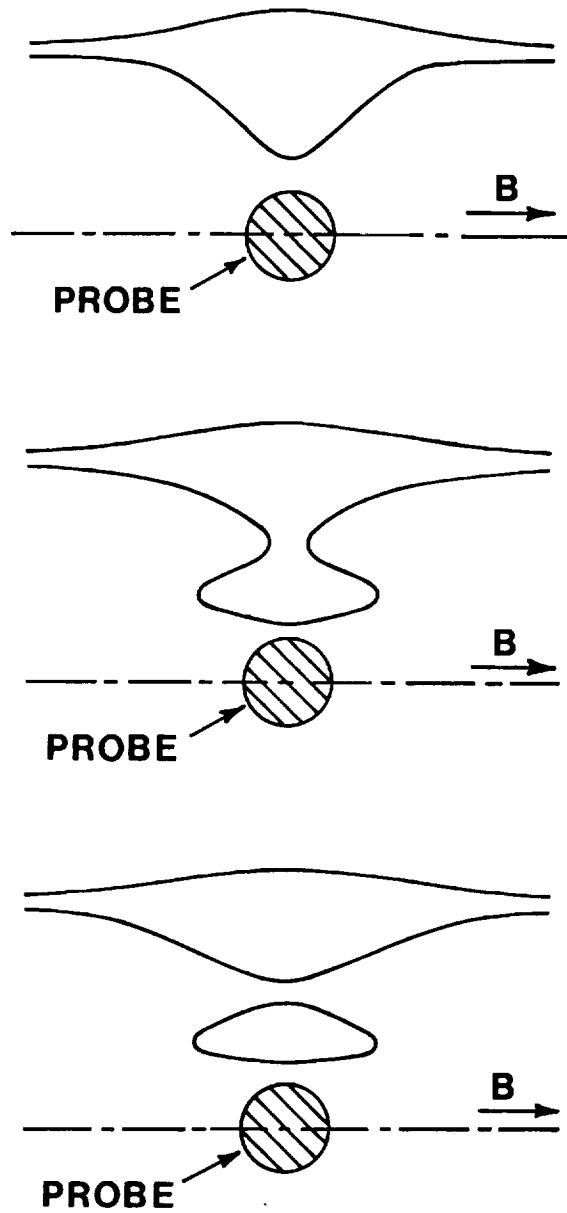
Figure 15. Development of "bulges" and disjoint "bubble" regions in magnetic "bottles", as described in Section 5.
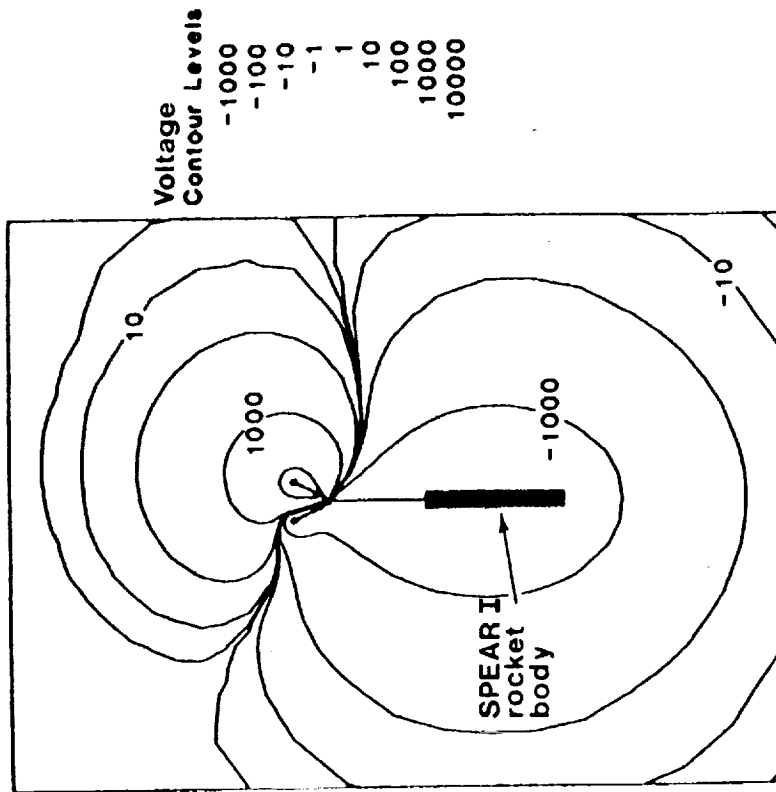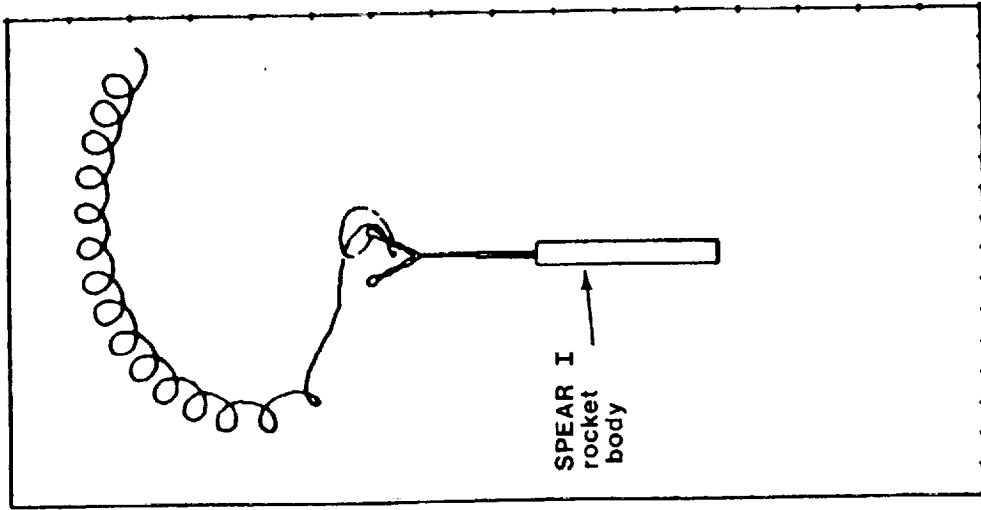
Figure 16(b). Reproduced from Fig. 8b of Katz et al (1989), showing the path of an electron in the potential distribution shown in Fig. 16(a). Note that the path is dramatically influenced by the presence of the ion-attracting sheath around the rocket body. Note also the sudden transition from "E × B drifting" motion to "accelerated" motion, and subsequent limiting of this motion by angular-momentum effects (Section 6).

SPEAR I
rocket
body

Voltage
Contour Levels

-1000
-100
-10
-1
1
10
100
1000
10000

10
1000
-1000
-10

SPEAR I
rocket
body

Figure 16(a). Reproduced from Fig. 8a of Katz et al (1989), showing SPEAR I potential contours calculated by the NASCAP/LEO simulation program for the case with one sphere biased to 46kV and the spacecraft ground at −6kV.
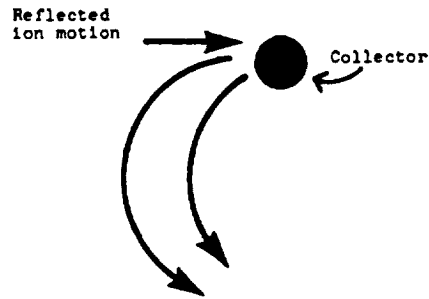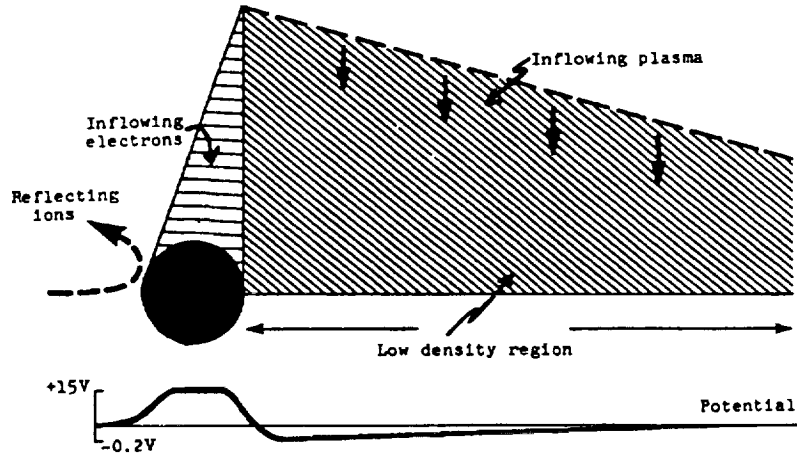
Figure 17. Reproduced from Figure 2 of Thompson (1985), showing the structure of the disturbed region around a large sphere in a drifting magnetoplasma.